THE HYPERBOLIC MONGE-AMPÈRE EQUATION ON A CYLINDER: WELL-POSEDNESS AND STABILITY

MARIA DELIYIANNI AND SHANKAR C. VENKATARAMANI

ABSTRACT. This paper develops a rigorous analytic framework for the hyperbolic Monge-Ampère equation on strip-like domains, which model wrinkled patterns in thin elastic sheets. Our work addresses the rigid side of the classical rigidity-flexibility dichotomy by defining this regime not by high smoothness, but by the more fundamental property of partial convexity. The hodograph transformation is the natural tool for this setting, as its validity is predicated on partial convexity. It converts the nonlinear Monge-Ampère equation into a linear damped wave equation, allowing us to formulate a well-posed Cauchy-Goursat problem. A key challenge is the corner singularity that arises where characteristic and non-characteristic boundary data meet. To resolve this, we develop a parametrix-corrector decomposition that captures the solution's inherent singular behavior. This method recasts the problem as a singular Volterra integral equation, for which we prove the existence and uniqueness of a new class of hodograph weak solutions. Finally, we derive energy estimates to establish the quantitative stability of these rigid solutions under perturbations of the underlying curvature function.

Contents

1. Introduction	2
2. Problem Formulation and Rigidity	5
2.1. Geometric Setting and Problem Formulation	5
2.2. Classical Solutions and Rigidity	5
3. The Hodograph Formulation	6
3.1. Exterior Differential System and Characteristics	7
3.2. The Linear PDE from the Hodograph Transformation	8
3.3. Non-integrability and the Goursat Problem	8
4. Symmetric Solutions and Problem Formulation	9
4.1. Symmetries and Inflection Lines	10
4.2. Smooth Gluing of Symmetric Solutions	10
4.3. Implications for the Goursat and Cauchy Problems	11

Date: October 1, 2025.

²⁰²⁰ Mathematics Subject Classification. 35L70, 53A05, 35L20, 45D05, 35Q74.

Key words and phrases. Hyperbolic Monge–Ampère equation, Cauchy-Goursat problem, Volterra equations, prescribed Gauss curvature.

This paper is dedicated to Professor Peter Constantin on the occasion of his 75th birthday with gratitude for his generosity, mentorship, guidance, and support.

5. The Well-Posed Cauchy–Goursat Problem	12
5.1. Problem Formulation	12
5.2. Existence and Uniqueness of Hodograph Weak Solutions	19
6. Singularities and Their Resolution	25
6.1. Asymptotic Analysis near a Goursat Boundary	27
6.2. The Parametrix and Corrector Solutions	28
6.3. Existence and Uniqueness for the Corrector	32
6.4. The Inverse Problem and Fold Singularities	34
7. Energy Estimates and Stability for the Cauchy–Goursat Problem	35
7.1. Energy Identity and Estimates	35
7.2. Stability under Perturbations of the Curvature Function	37
8. Conclusions and Future Directions	39
Acknowledgments	41
References	41

1. Introduction

The intricate, frilly patterns of leaves, fungi, and marine invertebrates are striking examples of hyperbolic geometry in nature [27, 29, 17]. These complex, multi-scale wrinkled shapes arise in thin elastic sheets when non-uniform growth or stress induces an intrinsic metric with negative Gaussian curvature [29]. The mathematical description of these surfaces often leads to the Hyperbolic Monge–Ampère equation, the prescribed Gauss curvature equation for isometric immersions of surfaces with negative curvature [26, 32]. While central to differential geometry and nonlinear analysis, in our context this equation presents a fundamental puzzle—the rigidity-flexibility dichotomy [13].

On one hand, classical results in differential geometry establish that smooth (C^2) isometric immersions of hyperbolic surfaces are rigid [10]; isometric immersions of large domains necessarily develop large curvatures and incur a prohibitive energetic cost. This mathematical rigidity seems to contradict the existence of the floppy, intricately wrinkled structures seen in nature [27, 35]. Our recent work has shed some light on this issue by considering a "flexible" regime of less-smooth surfaces [13, 14, 30, 35]. By introducing topological defects known as branch points, surfaces of class $C^{1,1}$ can form complex, lower-energy wrinkling patterns, providing an avenue for flexibility that nature appears to exploit [35].

Our work is just one aspect of the "flexible" side of the dichotomy. Flexibility itself has been revealed to be a spectrum of behaviors that depends on the precise regularity of the surface. At one extreme lies the foundational Nash-Kuiper theorem on C^1 isometric embeddings [20, 25], which established a paradigm of maximal flexibility by constructing an abundance of highly wrinkled solutions to the isometric immersion problem. The modern exploration of this spectrum, particularly on the intermediate $C^{1,\alpha}$ Hölder

scale, has been driven by the theory of convex integration [11, 15, 31]. This framework has been successfully applied to the isometric immersion problem and the associated Monge–Ampère system by a community of researchers including Borisov [3], Conti, DeLellis and Székelyhidi [8], and, Lewicka and Pakzad [21, 22, 23], leading to the construction of families of "wild" $C^{1,\alpha}$ isometries, that are candidates for weak solutions of the associated Monge–Ampére system [7, 6].

Within this spectrum of flexibility, our prior work has identified the $C^{1,1}$ class as particularly relevant to physical systems. Unlike the less regular $C^{1,\alpha}$ solutions ($\alpha < 1$), $C^{1,1}$ surfaces possess a well-defined bending energy [24], providing a potential energetic selection principle for the specific patterns observed in nature. Just as $C^{1,1}$ surfaces are, in a sense, "borderline" flexible, our work in this paper looks at the complementary problem of characterizing hyperbolic surfaces that are borderline rigid. We focus on the rigid regime by analyzing the structure and stability of partially convex solutions, where flexibility is suppressed. The manifestation of rigidity in highly smooth (C^3) solutions is a transport law that dictates that the wrinkling wavelength cannot change in the transverse direction. This law rules out the possibility of multi-generational sub-wrinkling and implies that a curvature component must maintain a definite sign between lines of inflection. We interpret this transport law not as an impediment, but as the very definition of the rigid solutions we seek to construct. The central goal of this paper is to characterize this regime by replacing the overly restrictive C^3 smoothness condition with the more fundamental property that defines rigidity in this setting: partial convexity. Classical C^3 solutions exhibit a rigid structure composed of regions of partial convexity (where w_{xx} has a definite sign), separated by non-bifurcating lines of inflection. Our approach is designed to formalize and extend this picture, capturing a broader class of solutions that retain this fundamental geometric character: a mosaic of partially convex patches glued together along well-behaved interfaces.

To analyze this structure, we study periodic solutions on a cylindrical domain $S^1 \times I$, where $I \subseteq \mathbb{R}$ is an interval (possibly unbounded), x is a coordinate along the compact periodic direction (the fibers) and the transverse coordinate, y, acts as a time-like variable. The problem can thus be viewed as a "1+1" dimensional hyperbolic system describing the evolution of periodic profiles in "time." In this context, the hodograph transformation, which exchanges the spatial variable $x \in S^1$ with its corresponding slope $p = w_x$, is the natural analytical tool, as its validity is predicated on the very condition of partial convexity ($w_{xx} \neq 0$). This transformation converts the nonlinear Monge–Ampère equation,

(1.1)
$$w_{xx}w_{yy} - w_{xy}^2 = -\lambda(y)^2,$$

into a linear damped wave equation [9]. This structure allows us to define our central object of study: $hodograph \ weak \ solutions$. This notion, which is based on an integral identity in the transformed (p, y) hodograph plane,

is distinct from the classical Alexandrov theory for elliptic problems [1]. It is specifically adapted to the symmetries of our problem and is designed to capture precisely the class of rigid solutions built from partially convex patches.

This framework leads naturally to the formulation of a Cauchy-Goursat problem [9]. However, a key difficulty arises from the geometry of this problem, the $corner\ singularity$ where non-characteristic Cauchy data meets characteristic Goursat data. As we argue below, standard notions of C^k compatibility for the boundary data are insufficient. Indeed, even a solution that is perfectly smooth in the original (x,y) variables will naturally generate inverse square-root singularities in its derivatives on the boundary of the hodograph domain, corresponding to cusps. We therefore introduce a more suitable notion of $weak\ compatibility$, which correctly captures the minimal regularity required for a well-posed Cauchy-Goursat problem.

Our primary contribution is the resolution of this singular problem, which we analyze in two distinct settings. For a finite cylinder, the problem is regularized and shown to be equivalent to a standard Volterra integral equation with a bounded kernel, for which well-posedness follows from classical theory [33]. The more challenging case is the semi-infinite cylinder, which corresponds to a pure Goursat problem with discontinuous boundary data at the origin. Herein lies the main technical novelty of our work: the development of a custom parametrix-corrector decomposition. The parametrix plays a dual role. First, it is constructed to account for the discontinuity in the Goursat data, reducing the problem to a singular Volterra equation for a more regular corrector term. The kernel of this equation exhibits a homogeneity of -1; consequently, the associated integral operator is not immediately seen as compact [19] on standard function spaces like Hölder or Sobolev spaces (the Hilbert transform being a classic example), meaning well-posedness requires a bespoke argument exploiting the specific structure of the kernel. Second, the parametrix provides the correct analytical structure for a higher-regularity theory. By explicitly subtracting the inherent singular behavior, it allows one to formulate meaningful compatibility conditions on the *corrector* rather than on the full solution. Finally, we construct an energy framework to derive quantitative stability estimates, demonstrating the continuous dependence of solutions on the underlying curvature function $\lambda(y)$.

The paper is organized as follows. In Section 2, we define the geometric setting of the problem and derive the transport law that demonstrates the inherent rigidity of classical solutions. Section 3 introduces our primary analytical tool, the hodograph transformation, which linearizes the Monge-Ampère equation. In Section 4, we leverage solution symmetries to reduce the problem to a fundamental domain and formally set up the Cauchy-Goursat problem. The well-posedness of this problem is the focus of Section 5, where we establish existence for the finite cylinder before developing a parametrix-corrector decomposition to resolve the boundary singularity that

arises in the more challenging semi-infinite cylinder case in Section 6. In Section 7, we construct an energy framework to prove quantitative stability estimates. We conclude in Section 8 with a summary and directions for future work.

2. Problem Formulation and Rigidity

2.1. Geometric Setting and Problem Formulation. To illustrate the geometry we will analyze, we first present a simple, explicit example of a surface with negative curvature that flattens at infinity. Consider the immersion given by a graph $(x, y) \mapsto (x, y, w(x, y))$ where

$$w(x,y) = e^{-y}\cos(x),$$

and whose Gaussian curvature is

$$K(y) = \frac{-e^{-2y}}{(1+e^{-2y})^2}.$$

The curvature K(y) depends only on the transverse variable y, highlighting a translation invariance in the x-direction. Furthermore, K(y) is strictly negative and decays to zero as $y \to \infty$, so the surface is negatively curved but becomes asymptotically flat. This example isolates the two key features that guide our analysis: localized negative curvature and a strip geometry where curvature depends only on the transverse variable and thus has a translation invariance "along the strip".

The above discussion motivates the general class of strip-like geometries we study. Metrics of the form

$$ds^2 = (1 + f(y))^2 dx^2 + dy^2$$

capture these same features. The Gaussian curvature for this metric is K(y) = -f''(y)/(1+f(y)). In the small deformation limit where $|f| \ll 1$, this simplifies to $K \approx -f''(y)$. We thus define the curvature via

$$K(y) = -\lambda(y)^2$$
 with $\lambda(y)^2 := f''(y)$,

referring to λ as the curvature function. With this notation, the immersion function w(x,y) satisfies the hyperbolic Monge–Ampère equation (1.1). We focus on solutions that are periodic in the x-direction, which naturally leads to considering domains that are topologically cylinders, such as $S^1 \times [l, L]$ or $S^1 \times [0, \infty)$. For the stability estimates developed later in the paper, we will assume a controlled decay of the curvature, for example, by requiring that the logarithmic derivative $\lambda_y/\lambda \leq -m_0 < 0$, remains negative and bounded away from zero for large y.

2.2. Classical Solutions and Rigidity. Before introducing the hodograph framework, it is important to understand the rigidity imposed by the Monge–Ampère equation on classical solutions. A natural starting point is to seek C^3 (or smoother) solutions w(x, y). However, the structure of the equation imposes a strong constraint that prevents refinement of oscillatory behavior,

ruling out physically observed phenomena [27, 28, 29]. This rigidity can be seen by differentiating the Monge–Ampère equation (1.1) with respect to x, which yields the conservation law:

$$(2.1) w_{xxx}w_{yy} + w_{xx}w_{xyy} - 2w_{xxy}w_{xy} = 0.$$

This equation implies a remarkable property: the level sets of the curvature component w_{xx} are transported along a vector field that is transverse to the fibers y = constant. To see this, define a vector field \mathbf{v} by

$$\mathbf{v} = -\frac{w_{xy}w_{yy}}{2\lambda(y)^2}\frac{\partial}{\partial x} + \frac{\partial}{\partial y}.$$

A direct computation of $\mathbf{v} \cdot \nabla w_{xx}$, in conjunction with (2.1), yields

(2.2)
$$\mathbf{v} \cdot \nabla(w_{xx}) = \left(\frac{w_{xy}w_{xyy} - 2w_{yy}w_{xxy}}{2\lambda(y)^2}\right)w_{xx}.$$

This demonstrates that $\mathbf{v} \cdot \nabla(w_{xx}) = \alpha(x,y)w_{xx}$ for some function $\alpha(x,y)$. In particular, the sign of w_{xx} does not change along the orbits of \mathbf{v} . This transport law reveals an inherent rigidity, which precludes multi-generational wrinkling and ensures that partial convexity is preserved as the solution evolves in the time-like variable y. This motivates the development of an analytical framework specifically designed to construct and characterize solutions within the rigid regime.

3. The Hodograph Formulation

The rigidity of classical solutions, as demonstrated by the transport law (2.2) in the physical (x,y) coordinates, motivates a change of framework. To analyze the structure of partially convex solutions, we employ the hodograph transformation. This is a classic technique for linearizing certain nonlinear hyperbolic systems by interchanging dependent and independent variables. Examples include its application to gas dynamics and to the Born-Infeld equation from nonlinear electrodynamics, both of which are treated in detail by Whitham [34] (Chapters 6 and 17, respectively). In our setting, this transformation similarly exchanges x (corresponding to the compact 'spatial' direction) with slope variables $p = w_x$, revealing the underlying linear nature of the Monge-Ampère equation.

The analysis is simplified by reparametrizing the transverse coordinate interpreted as time. We introduce the new variable u defined in terms of the curvature function $\lambda(y)$:

(3.1)
$$u(y) = \int_{y}^{\infty} \lambda(\eta) \, d\eta.$$

In the case of an infinite cylinder, the far-field limit $y \to \infty$ corresponds to $u \to 0$. For convenience, we will often treat λ as a function of u, denoting the composition $\lambda(y(u))$ simply as $\lambda(u)$. To avoid ambiguity in what follows, we adopt the convention that the prime notation refers exclusively to

differentiation with respect to u, so that

$$\lambda' \equiv \frac{d\lambda}{du} = -\frac{1}{\lambda} \frac{d\lambda}{dy} = -\frac{d}{dy} (\log \lambda).$$

3.1. Exterior Differential System and Characteristics. The language of Exterior Differential Systems (EDS) provides a powerful geometric approach to analyzing PDEs, where the equation is recast as a system of differential forms on a jet bundle [5, 18]. Fundamental results in this area, such as the Cartan–Kähler theorem, constitute a "formal theory" that can guarantee the existence of local, analytic solutions under certain involutivity conditions [2]. However, this formal theory does not by itself address the global existence and uniqueness for a specific boundary value problem like the one we study. Our aim here is therefore not to apply the full Cartan–Kähler machinery, but to use the geometric insight from the EDS framework to derive an equivalent linear PDE. This linear equation is the key to the rigorous, global analysis that follows.

To formulate the hyperbolic Monge–Ampére equation as an EDS, we consider the first jet bundle, $J^1(\Omega)$, over the domain $\Omega \subset \mathbb{R}^2$. This space formalizes the geometry by including not only the base coordinates but also the function's value and its first derivatives. A point in $J^1(\Omega)$ is given by the coordinates (x, y, w, p, q), which correspond to the location $(x, y) \in \Omega$, the value of the immersion $w: \Omega \to \mathbb{R}$, and the partial derivatives $p = w_x$ and $q = w_y$. The EDS for the Monge–Ampère equation is generated by the contact 1-form θ and the 2-form ω [18]:

(3.2)
$$\theta = dw - p \, dx - q \, dy$$
$$\omega = dp \wedge dq + \lambda^2 dx \wedge dy.$$

To adapt the system to characteristic variables, we recall from (3.1) that the differential relationship is $du = -\lambda dy$. With this change of variables, the forms can be combined into the following identity, which reveals the characteristic structure of the system:

$$\omega \pm \lambda(u)d\theta = (dp \mp du) \wedge (dq \pm \lambda(u) dx).$$

This factorization shows that the original system yields two characteristic subsystems [18]. To make this structure explicit, we introduce the characteristic coordinates $s = \frac{1}{2}(u+p)$ and $t = \frac{1}{2}(u-p)$. In these variables, the subsystems are defined by the Pfaffian equations with $\lambda(u) = \lambda(s+t)$:

$$(3.3) dt = 0, dq - \lambda(u) dx = 0,$$

$$(3.4) ds = 0, dq + \lambda(u) dx = 0.$$

From these relations, we can extract a more compact formulation that will be central in what follows. Specifically, along any path we have

$$dq = \lambda(u)(\mu ds - \nu dt), \quad dx = \mu ds + \nu dt,$$

where we define $\mu = \frac{\partial x}{\partial s} = x_s$ and $\nu = \frac{\partial x}{\partial t} = x_t$. Since q is a function of s and t, its exterior derivative must vanish, namely d(dq) = 0. This implies

$$d\bigg(\lambda(u)\left(\frac{\partial x}{\partial s}\,ds - \frac{\partial x}{\partial t}\,dt\right)\bigg) = 0.$$

Thus, solving the Monge–Ampère equation becomes equivalent to finding a function x(s,t) such that the 1-form

(3.5)
$$\alpha = \lambda(s+t)(x_s ds - x_t dt)$$

is exact $(d\alpha = 0)$. By Stokes' theorem, this is equivalent to requiring that $\oint_C \alpha = 0$ for any closed contour C.

3.2. The Linear PDE from the Hodograph Transformation. For the 1-form $\alpha = P ds + Q dt$ to be exact, its components must satisfy the compatibility condition

$$\frac{\partial Q}{\partial s} = \frac{\partial P}{\partial t}.$$

From (3.5) we have $P = \lambda x_s$ and $Q = -\lambda x_t$. Denoting $\lambda = \lambda(s+t)$ and $\lambda' = \frac{d\lambda}{d(s+t)}$, we compute:

$$\frac{\partial P}{\partial t} = \frac{\partial}{\partial t} (\lambda x_s) = \lambda' x_s + \lambda x_{st},$$

$$\frac{\partial Q}{\partial s} = \frac{\partial}{\partial s} (-\lambda x_t) = -\lambda' x_t - \lambda x_{st}.$$

Equating the two derivatives gives

$$(3.6) -\lambda' x_t - \lambda x_{st} = \lambda' x_s + \lambda x_{st}.$$

Let us introduce the linear operator

(3.7)
$$L[x] := 2\lambda x_{st} + \lambda'(x_s + x_t).$$

Rearranging terms in (3.6) leads to the linear PDE for x(s,t):

$$(3.8) L[x] = 0.$$

If $\lambda \neq 0$, we can also write this as:

$$(3.9) x_{st} + \frac{\lambda'}{2\lambda}(x_s + x_t) = 0$$

This PDE describes functions x = x(s,t) satisfying the requirement that the one form α is exact.

3.3. Non-integrability and the Goursat Problem. At first glance, one might expect the situation to parallel the wave equation: once the characteristic structure is revealed, one could integrate along characteristics to obtain explicit formulas for the solution, as in d'Alembert's formula. This would correspond to the system being *Darboux integrable* [18], meaning that the characteristic equations admit Riemann invariants constant along characteristics. However, for the Monge–Ampère equation (1.1), this is generally not the case, as the following lemma shows.

Lemma 3.1. The characteristic subsystems (3.3) and (3.4) are Darboux integrable if and only if the function $\lambda(u)$ is constant.

Proof. For the system to be Darboux integrable, each characteristic subsystem should be Frobenius, i.e., for i = 1, 2, we should not get any additional conditions, beyond $\beta_i = 0, \zeta_i = 0$ by prolongation (differentiation) [5]. In other words $d\beta_i$ and $d\zeta_i$ should be in the ideal generated by β_i and ζ_i . Let us check this for subsystem 2. We have

$$d\beta_2 = d(ds) = 0,$$

$$d\zeta_2 = d(dq + \lambda(u) dx) = d\lambda(u) \wedge dx = \lambda'(u) du \wedge dx.$$

It is clear that $d\beta_2$ lies in the ideal. For $d\zeta_2$, Frobenius integrability requires $d\zeta_2 \wedge \beta_2 \wedge \zeta_2 = 0$. We compute:

$$d\zeta_2 \wedge \beta_2 \wedge \zeta_2 = (\lambda'(u) du \wedge dx) \wedge ds \wedge (dq + \lambda(u) dx)$$
$$= \lambda'(u) du \wedge dx \wedge ds \wedge dq.$$

Since u = s + t, we have du = ds + dt, and hence the above becomes

$$\lambda'(s+t)(ds+dt) \wedge dx \wedge ds \wedge dq = \lambda'(s+t)dt \wedge dx \wedge ds \wedge dq.$$

This 4-form vanishes if and only if $\lambda'(u) \equiv 0$, i.e. $\lambda(u)$ is constant. Otherwise, the subsystem (3.4) is not involutive and thus not Darboux integrable. A similar calculation applies to (3.3). Therefore the Monge–Ampère system (3.2) is neither Darboux integrable nor even semi-integrable.

The failure of Darboux integrability confirms that no simple d'Alemberttype formula is available for the general case. We therefore turn from seeking explicit formulas to analyzing a well-posed boundary value problem. For a hyperbolic PDE expressed in characteristic coordinates, such as Equation (3.9), the *Goursat problem*, where data is prescribed on two intersecting characteristic curves, provides a fundamental and well-posed framework. This formulation is particularly well-suited for our analysis because, as we will show, it can be converted directly into a Volterra integral equation. This integral representation will become the central tool for constructing and analyzing solutions in the sections that follow.

4. Symmetric Solutions and Problem Formulation

While the hodograph formulation linearizes the Monge–Ampère equation, it applies only on domains where the solution is partially convex $(w_{xx} \neq 0)$. For periodic solutions, it is of course impossible to have $w_{xx} \neq 0$ everywhere on a compact fiber y = constant. Consequently, the domains of partial convexity appear as patches bounded by lines of inflection $w_{xx} = 0$. To construct a global solution, one must analyze the solution on a fundamental patch and understand how to glue it to its neighbors. The properties of this gluing are determined by the symmetries of the solution.

In this section, we show how symmetry provides the geometric framework for formulating the problem. Certain exact solutions exhibit strong reflectional and translational symmetries. These symmetries fix the location of inflection lines and determine how adjacent solution patches can be joined. By analyzing this class of symmetric solutions, we obtain the natural boundary configuration that motivates the Cauchy–Goursat formulation studied in the next section.

- 4.1. Symmetries and Inflection Lines. We are motivated by the structure of the exact product solution $w(x,y) = e^{-y}\cos(x)$ of (1.1). This example suggests looking at a class of solutions w(x,y) that share its key symmetries:
 - (1) Even under reflection about x = 0: The solution is even in x,

$$w(-x,y) = w(x,y).$$

(2) **Odd under translation by a half-period:** The solution is antisymmetric under a shift by half its period, which we take to be π ,

$$w(x + \pi, y) = -w(x, y).$$

The second condition implies periodicity with period 2π . Taken together, these symmetries fix the location of the inflection lines.

Lemma 4.1. If w(x,y) is C^2 and satisfies the two symmetry conditions above, then it has lines of inflection at $x = \pm \frac{\pi}{2}$.

Proof. The translational anti-symmetry implies a corresponding anti-symmetry for the second derivative, $w_{xx}(x+\pi,y) = -w_{xx}(x,y)$. The reflectional symmetry implies that w_{xx} is even, $w_{xx}(-x,y) = w_{xx}(x,y)$.

Evaluating the first identity at $x = -\frac{\pi}{2}$ gives

$$w_{xx}(\frac{\pi}{2}, y) = -w_{xx}(-\frac{\pi}{2}, y).$$

From the second identity we know $w_{xx}(-\frac{\pi}{2},y) = w_{xx}(\frac{\pi}{2},y)$. Substituting this relation yields

$$w_{xx}(\frac{\pi}{2}, y) = -w_{xx}(\frac{\pi}{2}, y).$$

Hence $2w_{xx}(\frac{\pi}{2},y)=0$, so $w_{xx}(\frac{\pi}{2},y)=0$. By the even symmetry of w_{xx} , it must also vanish at $x=-\frac{\pi}{2}$.

4.2. Smooth Gluing of Symmetric Solutions.

Theorem 4.2 (C^{∞} Gluing). Assume $\lambda(y)$ is C^{∞} and let w(x,y) be a C^{∞} solution on a fundamental patch $x \in [-x_+, x_+]$ that is even in x. Then the anti-symmetric extension defined by $w(x + 2x_+, y) = -w(x, y)$ yields a globally C^{∞} periodic solution.

Proof. For the extended function to be C^{∞} , all of its derivatives must be continuous at the gluing boundaries, e.g., at $x = x_{+}$. The anti-symmetric

extension rule implies that, for the n-th derivative to be continuous, it must satisfy the gluing condition:

$$\lim_{x \to x_+^+} w^{(n)}(x,y) = -w^{(n)}(x_+ - 2x_+, y) = -w^{(n)}(-x_+, y).$$

The symmetry of the solution on the patch, w(x,y) = w(-x,y), implies that its *n*-th derivative has a definite symmetry: $w^{(n)}(-x_+,y) = (-1)^n w^{(n)}(x_+,y)$. Substituting this into the gluing condition gives the requirement for continuity of the *n*-th derivative:

$$w^{(n)}(x_+, y) = -[(-1)^n w^{(n)}(x_+, y)] = (-1)^{n+1} w^{(n)}(x_+, y).$$

We examine this condition separately for even derivatives (n even) and odd derivatives (n odd):

- Even derivatives: The condition becomes $w^{(n)}(x_+, y) = -w^{(n)}(x_+, y)$, which implies $w^{(n)}(x_+, y) = 0$. Thus, for smooth gluing to be possible, all even-order x-derivatives of the solution must vanish at the inflection points.
- Odd derivatives: The condition becomes $w^{(n)}(x_+, y) = w^{(n)}(x_+, y)$. This is always true and imposes no further constraints.

A solution that is even and arises from a separable product form, such as $w(x,y) = g(y)\cos(kx)$, automatically satisfies the condition that all its even x-derivatives (which are proportional to $\cos(kx)$) vanish at the inflection points $x_+ = \pi/(2k)$. The same reasoning applies to all mixed derivatives $\partial_y^m \partial_x^n w$ due to the smoothness of $\lambda(y)$. Therefore, the gluing is not just C^2 or C^3 , but smooth to all orders, yielding a global C^∞ solution.

4.3. Implications for the Goursat and Cauchy Problems. The geometric properties of this symmetric class of solutions directly motivate the boundary value problems analyzed in the remainder of this paper. In particular, the location of inflection lines and the role of symmetry provide the natural boundary framework for both Goursat and Cauchy formulations.

The Goursat Problem. The fixed inflection lines at $x=\pm\frac{\pi}{2}$ naturally define a fundamental solution patch, like the concave region where $w_{xx}<0$ on the physical domain $x\in[-\frac{\pi}{2},\frac{\pi}{2}]$. In the hodograph plane, these inflection lines correspond to the boundaries of the domain for the function x(s,t). This motivates the choice of Goursat boundary conditions used in the parametrix construction and in analyzing the singular problem at the origin:

$$x_{\pm} = \pm \frac{\pi}{2}.$$

The Cauchy Problem. The Cauchy data for the physical problem is typically imposed at a "remote" boundary, such as a line of constant y = L. Recalling the potential coordinate u from (3.1), we note that the far field in physical space corresponds to the near field in hodograph space: as $y \to \infty$, one has $u \to 0^+$. A large but finite y = L corresponds to a small positive

value of the time-like variable, c = u(L). Therefore, the physical Cauchy problem for w at large y becomes the initial value problem for x at small u. For consistency with the global structure, we assume that any prescribed Cauchy data for w and w_y at y = L also respect the symmetry conditions.

5. The Well-Posed Cauchy-Goursat Problem

Before analyzing the full singular problem at the origin, we first establish well-posedness on a regularized domain where the corner is truncated. This leads to the *Cauchy–Goursat problem*, a mixed initial-boundary value problem for hyperbolic PDEs [9] in which part of the boundary is non-characteristic (Cauchy data) and part is characteristic (Goursat data). Such structures naturally arise in physical models: the Cauchy problem prescribes initial data on a spacelike curve, while the Goursat problem prescribes boundary data along (possibly intersecting) characteristic curves, such as the edges of a light cone.

In this section, we formulate the problem and clarify the compatibility requirements on the boundary data. We then prove uniqueness of classical solutions via contour integration, analyze the geometric cases, and unify them into a single Volterra-type integral equation. Finally, we extend this framework to weak solutions, establishing existence, uniqueness, and precise attainment of the prescribed boundary data [9, 33].

5.1. **Problem Formulation.** We define the domain of interest as follows:

- (5.1) For a constant c > 0, let $\Omega = \{(s,t) \in \mathbb{R}^2 \mid s > 0, t > 0, s + t > c\}$, which we refer to as the *finite-cylinder domain*. The boundary $\partial\Omega$ of this domain's closure is composed of three segments:
 - A non-characteristic (Cauchy) segment: $\Gamma_C = \{(s,t) \mid s+t=c, s \geq 0, t \geq 0\};$
 - Two characteristic (Goursat) segments: $\Gamma_1 = \{(s,0) \mid s \geq c\}$ and $\Gamma_2 = \{(0,t) \mid t \geq c\}$.

This setup showcases the interaction between the Cauchy line, where data is specified in a non-characteristic fashion, and the Goursat segments, which are characteristic boundaries. Together they form a truncated cone that avoids the singular corner, as shown in Figure 1.

On these boundary segments, we prescribe the following data:

$$x(s,0) = g(s) \quad \text{for } s \ge c \text{ (on } \Gamma_1)$$

$$x(0,t) = h(t) \quad \text{for } t \ge c \text{ (on } \Gamma_2)$$

$$x(s,c-s) = f(s) \quad \text{for } 0 \le s \le c \text{ (on } \Gamma_C)$$

$$(5.2) \qquad (\partial_s + \partial_t)x(s,c-s) = n(s) \quad \text{for } 0 \le s \le c \text{ (on } \Gamma_C).$$

Here, $\partial_s + \partial_t$ is the derivative normal to the Cauchy segment Γ_C .

It is important to emphasize that not every choice of boundary data $\{g, h, f, n\}$ yields a meaningful solution. In particular, at the corners (c, 0)

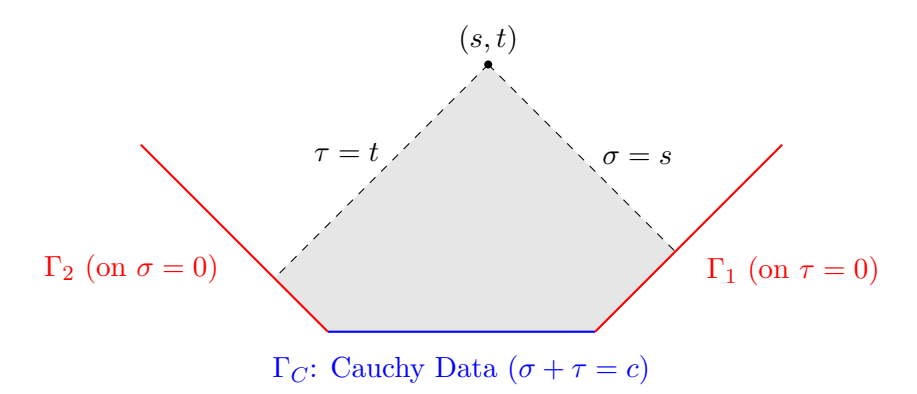


FIGURE 1. Geometry of the Cauchy–Goursat problem in rotated characteristic coordinates (σ, τ) . The shaded region shows the domain of dependence for (s, t).

and (0, c) the boundary conditions must align in a consistent way. To make this precise, we introduce compatibility notions, beginning with weak compatibility of the data.

Definition 5.1 (Weak compatibility for the Cauchy–Goursat data). The Cauchy–Goursat boundary data $\{g, h, f, n\}$ are weakly compatible if

- (1) $\{g, h, f\}$ are C^0 -compatible, meaning that there exists a C^0 function in a neighborhood of $\partial\Omega$ that agrees with the prescribed Dirichlet data on $\Gamma_1 \cup \Gamma_C \cup \Gamma_2$. This requires, at a minimum, that g(c) = f(c) and h(c) = f(0).
- (2) f is absolutely continuous, so that the tangential derivative is defined a.e. on Γ_C and is integrable, i.e., $f' \in L^1(\Gamma_C)$.
- (3) The prescribed normal derivative on Γ_C satisfies $n \in L^1(\Gamma_C)$.

These assumptions are deliberately weak: they guarantee continuity and integrability without enforcing strict derivative consistency. This flexibility allows us to capture weak solutions, without requiring agreement of derivatives such as g'(c), h'(c), f'(0), f'(c), the normal data n(0), n(c), or even their existence.

Having clarified the mildness of these requirements, we next specify what it means for a function to actually *attain* such weakly compatible data on the boundary.

Definition 5.2 (Attainment of boundary conditions). A continuous function $x \in C^0(\bar{\Omega})$, where $\bar{\Omega} = \Omega \cup \partial \Omega$, attains the weakly compatible Cauchy–Goursat boundary conditions $\{g, h, f, n\}$ if g, h, and f are equal to x restricted to the corresponding segments Γ_1, Γ_2 and Γ_C in $\partial \Omega$ and, for almost all $s \in [0, c]$, the limit

$$\lim_{z \to 0^+} \frac{x(s+z, c-s+z) - x(s, c-s)}{z}$$

exists and is equal to n(s).

The natural function space for solutions to the governing PDE is dictated by its structure. For what follows, we use the following definition for a classical solution of the Cauchy–Goursat problem: a function $x \in C^2(\Omega)$ that attains the boundary data $\{g,h,f,n\}$ are necessarily weakly compatible.

We are now ready to state the main theorem concerning the well-posedness of the Cauchy–Goursat problem for the specified hyperbolic equation.

Theorem 5.3. Let $\lambda \in C^1$ with $\lambda \neq 0$, and consider the hyperbolic equation

$$2\lambda(\sigma+\tau)x_{\sigma\tau} + \lambda'(\sigma+\tau)(x_{\sigma}+x_{\tau}) = 0$$

on the domain Ω with boundary $\partial \Omega = \Gamma_1 \cup \Gamma_2 \cup \Gamma_C$, and suppose that the Cauchy-Goursat boundary data $\{g, h, f, n\}$ are defined as above.

If x(s,t) is a classical solution and $(s,t) \in \overline{\Omega}$, the value x(s,t) is uniquely determined by an explicit integral relation depending only on the solution $x(\sigma,\tau)$ along the characteristics $\sigma=s$ and $\tau=t$ leading to (s,t), together with the prescribed boundary data on the portion of $\partial\Omega$ lying in the causal past of (s,t), namely on $\partial\Omega \cap [0,s] \times [0,t]$.

Proof. The key observation is that the PDE is equivalent to the exactness of the 1-form $\alpha = \lambda(\sigma + \tau)(x_{\sigma} d\sigma - x_{\tau} d\tau)$. Hence, the integral of α over any closed contour C must vanish, i.e., $\oint_C \alpha = 0$. The main step is to construct C carefully and, depending on the position of the point P(s,t), different contour shapes arise. These four cases are summarized in Figure 2, which will serve as the guiding diagrams throughout the proof.

In each case, the contour integrals naturally split into two parts: those involving the unknown function x along the characteristic segments leading to (s,t), and those lying entirely on the prescribed boundary (the blue curves in Figure 2), where the Cauchy–Goursat data determine the values. We will refer to these as the "unknown" and "known" contributions, respectively. For our analysis, we proceed by examining the four separately.

Case I: s > c and t > c. We choose a pentagonal contour C with vertices

$$P(s,t) \rightarrow A(s,0) \rightarrow B(c,0) \rightarrow D(0,c) \rightarrow E(0,t) \rightarrow P(s,t)$$

as illustrated in Figure 2(a).

The resulting integral equation for x is

$$\int_0^s \lambda(\sigma+t)x_{\sigma}(\sigma,t) d\sigma + \int_0^t \lambda(s+\tau)x_{\tau}(s,\tau) d\tau = -\mathcal{J}_1,$$

where

$$\mathcal{J}_1 = \int_s^c \lambda(\sigma) x_{\sigma}(\sigma, 0) d\sigma + \int_c^0 \lambda(c) n(\sigma) d\sigma - \int_c^t \lambda(\tau) x_{\tau}(0, \tau) d\tau.$$

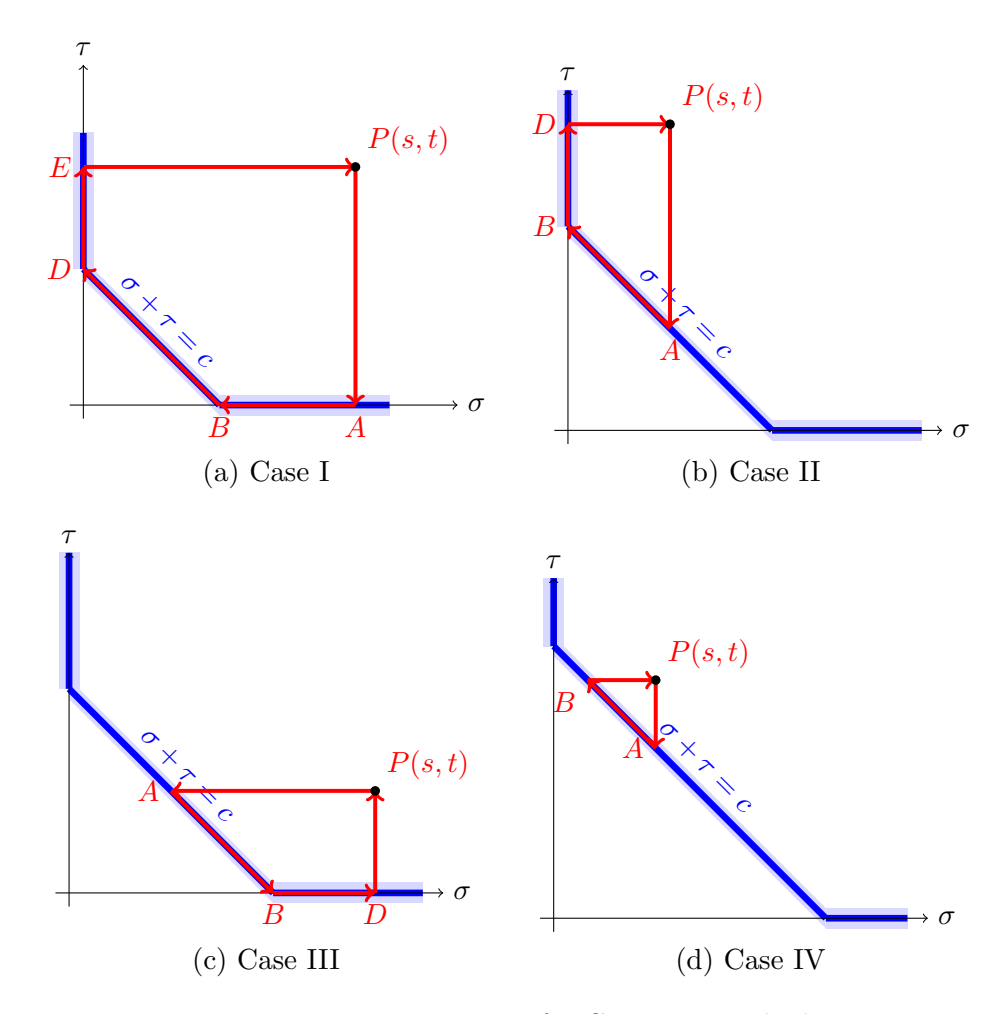


FIGURE 2. Integration contours for Cases I–IV. The known boundary is in blue.

Case II: $0 \le s \le c$ and t > c. We choose a quadrilateral contour C with vertices

$$P(s,t) \to A(s,c-s) \to B(0,c) \to D(0,t) \to P(s,t),$$

as illustrated in Figure 2(b).

The resulting integral equation for x is

$$\int_0^s \lambda(\sigma+t)x_{\sigma}(\sigma,t) d\sigma + \int_{c-s}^t \lambda(s+\tau)x_{\tau}(s,\tau) d\tau = -\mathcal{J}_2,$$

where

$$\mathcal{J}_2 = \int_s^0 \lambda(c) n(\sigma) d\sigma - \int_c^t \lambda(\tau) x_\tau(0, \tau) d\tau.$$

Case III: s > c and $0 \le t \le c$. By symmetry with Case II, we choose a quadrilateral contour C with vertices

$$P(s,t) \to A(c-t,t) \to B(c,0) \to D(s,0) \to P(s,t),$$

as illustrated in Figure 2(c).

The resulting integral equation for x is

$$\int_{c-t}^{s} \lambda(\sigma+t)x_{\sigma}(\sigma,t) d\sigma + \int_{0}^{t} \lambda(s+\tau)x_{\tau}(s,\tau) d\tau = -\mathcal{J}_{3},$$

where

$$\mathcal{J}_3 = \int_t^0 \lambda(c) n(c-\tau) d\tau + \int_c^s \lambda(\sigma) x_{\sigma}(\sigma,0) d\sigma.$$

Case IV: 0 < s < c, 0 < t < c, and s + t > c. We construct a triangular contour C with vertices

$$P(s,t) \to A(s,c-s) \to B(c-t,t) \to P(s,t),$$

as illustrated in Figure 2(d).

Rearranging terms from the vanishing integral condition gives

$$\int_{c-t}^{s} \lambda(\sigma+t)x_{\sigma}(\sigma,t) d\sigma + \int_{c-s}^{t} \lambda(s+\tau)x_{\tau}(s,\tau) d\tau = -\mathcal{J}_{4},$$

where

$$\mathcal{J}_4 = \int_c^{c-t} \lambda(c) n(\sigma) \, d\sigma. \qquad \Box$$

Remark 5.4. In the proof above, the quantities \mathcal{J}_i (i = 1, 2, 3, 4) arise as appropriate integrals along portions of the boundary $\partial\Omega$. These integrals involve the given Cauchy–Goursat boundary data $\{g, h, f, n\}$, defined in (5.2).

The relations obtained in **I**–**IV** share the same underlying structure. Our next step is to introduce a generalized contour that accommodates all four cases and unifies them into a single integral equation.

Proposition 5.5. The integral relations derived previously can be recast, via integration by parts, into a unified Volterra-type integral equation for the function x(s,t).

Proof. The partition of our domain Ω into four regions leads to integration contours with different numbers of vertices, depending on the region. In this case, a uniform treatment is achieved by defining a single, generalized pentagonal contour C whose vertices adapt to each case, where we allow for zero-length edges. Thus, using the notation $\xi^+ = \max(\xi, 0)$, the vertices of this contour are:

$$V_1 = ((c-t)^+, \min(c,t)), V_2 = (\min(c,s), (c-s)^+),$$

 $V_3 = (s, (c-s)^+), V_4 = (s,t),$
 $V_5 = ((c-t)^+, t).$

Invoking once again the exactness of the 1-form α , we deduce that integral of this form over this closed contour must vanish. Separating the "unknown" from the "known" boundary paths gives:

(5.3)
$$\int_{(c-t)^+}^s \lambda(\sigma+t)x_{\sigma}(\sigma,t) d\sigma + \int_{(c-s)^+}^t \lambda(s+\tau)x_{\tau}(s,\tau) d\tau = \mathcal{J}_5,$$

where \mathcal{J}_5 represents the sum of the integrals along the segments V_1V_2 , V_2V_3 , and V_5V_1 .

We now show that \mathcal{J}_5 is determined entirely by the prescribed initial and boundary data.

- The integral over V_1V_2 : lies on the line $\sigma+\tau=c$ and is determined by the Cauchy data.
- The integral along V_2V_3 : This path lies on the line $\tau = (c-s)^+$. If $s \leq c$, the path has zero length and the integral is trivially zero. If s > c, the path is the segment from (c,0) to (s,0), and the integral becomes $\int_c^s \lambda(\sigma)x_{\sigma}(\sigma,0)d\sigma$. This integrand here is known from the Goursat data prescribed on $\tau = 0$.
- The integral along V_5V_1 : This path is on the line $\sigma = (c-t)^+$. If $t \leq c$, the path has zero length and the integral is zero. If t > c, the path is from (0,t) to (0,c), and the integral becomes $-\int_c^t \lambda(\tau) x_{\tau}(0,\tau) d\tau$. This integrand is known from the Goursat data on $\sigma = 0$.

Equation (5.3), however, still contains derivatives of the unknown function x. To eliminate these and shift the derivatives from the unknown x onto the known coefficient λ , we apply integration by parts along the edges V_3V_4 and V_4V_5 . For clarity, consider a generic contour segment with endpoints (σ_0, τ) and (σ_1, τ) (or analogously (σ, τ_0) and (σ, τ_1) when integrating in τ). Integration by parts then yields the template identities:

$$\int_{\sigma_0}^{\sigma_1} \lambda(\sigma + t) x_{\sigma}(\sigma, t) d\sigma = \lambda(\sigma_1 + t) x(\sigma_1, t) - \lambda(\sigma_0 + t) x(\sigma_0, t)$$
$$- \int_{\sigma_0}^{\sigma_1} \lambda'(\sigma + t) x(\sigma, t) d\sigma,$$
$$\int_{\tau_0}^{\tau_1} \lambda(s + \tau) x_{\tau}(s, \tau) d\tau = \lambda(s + \tau_1) x(s, \tau_1) - \lambda(s + \tau_0) x(s, \tau_0)$$
$$- \int_{\tau_0}^{\tau_1} \lambda'(s + \tau) x(s, \tau) d\tau.$$

Thus, applying this procedure to the segments V_3V_4 and V_4V_5 and then collecting terms, yields the final and unified Volterra-type integral equation

for x(s,t):

$$2\lambda(s+t)x(s,t) = \int_{(c-t)^{+}}^{s} \lambda'(\sigma+t)x(\sigma,t) d\sigma + \int_{(c-s)^{+}}^{t} \lambda'(s+\tau)x(s,\tau) d\tau + \lambda(\max(c,t))x((c-t)^{+},t) + \lambda(\max(s,c))x(s,(c-s)^{+}) + \int_{(c-t)^{+}}^{\min(c,s)} \lambda(c)(x_{\sigma}+x_{\tau})|_{\sigma+\tau=c} d\sigma + \int_{\min(c,s)}^{s} \lambda(\sigma+(c-s)^{+})x_{\sigma}(\sigma,(c-s)^{+}) d\sigma + \int_{\min(c,t)}^{t} \lambda((c-t)^{+}+\tau)x_{\tau}((c-t)^{+},\tau) d\tau.$$
(5.4)

Lastly, we note that if $x: \Omega \to \mathbb{R}$ is a classical solution, this equation holds for any point (s,t) in the domain.

Among the resulting terms, those that depend only on the boundary data can be collected into a single quantity, denoted by $\mathcal{G}(s,t)$. In practice, to define this, we separate out these contributions, insert the boundary conditions from (5.2), and perform additional integrations by parts. Importantly, \mathcal{G} is determined entirely by the prescribed boundary data, independent of the interior values of x(s,t).

$$\mathcal{G}(s,t) = \begin{cases}
\lambda(c)f(s) & s \leq c, \\
2\lambda(s)g(s) - \lambda(c)g(c) - \int_{c}^{s} g(\sigma)\lambda'(\sigma) d\sigma & s > c
\end{cases}$$

$$+ \begin{cases}
\lambda(c)f(c-t) & t \leq c, \\
2\lambda(t)h(t) - \lambda(c)h(c) - \int_{c}^{t} h(\tau)\lambda'(\tau) d\tau & t > c
\end{cases}$$

$$+ \int_{(c-t)^{+}}^{\min(c,s)} \lambda(c)n(\sigma) d\sigma.$$
(5.5)

Remark 5.6. If the data $\{g, h, f, n\}$ is weakly compatible (see Definition 5.1), then the map

$$(s,t) \mapsto \int_{(c-t)^+}^{\min(c,s)} \lambda(c) n(\sigma) d\sigma$$

is continuous on Ω , since $\lambda(c)$ is a constant and $n \in L^1(\Gamma_c)$. It is also straightforward to verify that \mathcal{G} is continuous, particularly across the lines s = c and t = c. However, \mathcal{G} is in general not differentiable, even if the boundary data $\{g, h, f, n\}$ is C^k compatible for every k, i.e., obtained by restricting a C^k function defined on a neighborhood of $\partial\Omega$.

To see why, fix t > c and compute

$$\mathcal{G}_s(c^-,t) = \lambda(c) (f'(c) + n(c))$$
 and $\mathcal{G}_s(c^+,t) = 2\lambda(c)g'(c) - g(c)\lambda'(c)$.

While $\{g, h, f, n\}$ satisfy compatibility relations, the coefficient λ is independent. Thus $\lambda(c)$ and $\lambda'(c)$ are arbitrary, and differentiability across s = c would force the additional conditions f'(c) + n(c) - 2g'(c) = 0 and g(c) = 0. Since one may choose a C^k function x near $\partial\Omega$ with $g(c) = x(c, 0) \neq 0$, no k can guarantee that \mathcal{G} is C^1 .

5.2. Existence and Uniqueness of Hodograph Weak Solutions. We extend the analysis of the Cauchy–Goursat problem from classical to weak solutions on finite cylinders. The key observation is that the integral representation (5.4) remains valid when x is only continuous on $\bar{\Omega}$ (see (5.1)) This allows us to formulate a well-posed problem in a broader setting. We begin by defining what we mean by a hodograph weak solution, and then establish existence and uniqueness through the framework of two-dimensional Volterra integral equations [9, 33].

Definition 5.7 (Hodograph weak solution). A continuous function $x:\Omega\to\mathbb{R}$ is called a *hodograph weak solution* to the Cauchy–Goursat problem given by (3.9) and (5.2) if it satisfies the integral relation (5.4) at every point of $\bar{\Omega}$.

Having recast our PDE as the integral equation (5.4), we now turn to the question of existence and uniqueness of weak solutions. For this purpose, we fix a bounded rectangle $R = [0, S] \times [0, T] \subset \mathbb{R}^2$, and continuous functions $a: [0, T] \to [0, S]$ and $b: [0, S] \to [0, T]$. The integral relation (5.4) can be recast as a two-dimensional Volterra integral equation of the second kind [33], for which the following theorem applies.

Theorem 5.8. Let x satisfy the two-dimensional Volterra integral equation of the second kind

$$x(s,t) = \mathcal{F}(s,t) + \int_{a(t)}^{s} K_1(s,t,\sigma) x(\sigma,t) d\sigma + \int_{b(s)}^{t} K_2(s,t,\tau) x(s,\tau) d\tau,$$

for $(s,t) \in \Omega$. If the forcing term \mathcal{F} is continuous on Ω , and the kernels K_1, K_2 are continuous on the compact set

$$\{(s,t,\sigma,\tau)\mid (s,t)\in\Omega,\ a(t)\leq\sigma\leq s,\ b(s)\leq\tau\leq t\},$$

then there exists a unique continuous solution x on Ω .

Remark 5.9. For our setup, all four cases (see Figure 2) are covered by taking $a(t) = (c-t)^+$, $b(s) = (c-s)^+$, and making the identifications

(5.6)
$$\mathcal{F}(s,t) = \frac{\mathcal{G}(s,t)}{2\lambda(s+t)}, \ K_1(s,t,\sigma) = \frac{\lambda'(\sigma+t)}{2\lambda(s+t)}, \ K_2(s,t,\tau) = \frac{\lambda'(s+\tau)}{2\lambda(s+t)},$$

where \mathcal{G} is defined in (5.5). Note that K_1 and K_2 are not bounded on the full domain $0 \le \sigma \le S$, $0 \le \tau \le t \le T$, since for instance, they diverge

along $\sigma = s$ as $s + t \to 0$. To avoid this singular behavior at the origin, we (initially) restrict attention to compact subdomains of $R \setminus \{\mathbf{0}\}$, such as the truncated-cylinder domain Ω (see (5.1)). Here and henceforth, we will denote the origin (0,0) by $\mathbf{0}$.

Proof. The proof proceeds by the method of successive approximations [19].

Setup: We work in the Banach space $C(\Omega)$ of continuous functions on the compact domain Ω , equipped with the supremum norm $\|\cdot\|_{\infty}$. Define the operator $\mathcal{A}: C(\Omega) \to C(\Omega)$ by (5.7)

$$(\mathcal{A}x)(s,t) = \mathcal{F}(s,t) + \int_{a(t)}^{s} K_1(s,t,\sigma) x(\sigma,t) d\sigma + \int_{b(s)}^{t} K_2(s,t,\tau) x(s,\tau) d\tau.$$

Since f, K_1 , K_2 , a, and b are continuous and Ω is compact, their domains of definition are compact as well. In particular, K_1 and K_2 are bounded, so \mathcal{A} maps continuous functions to continuous functions. We also define the Volterra operator

(5.8)
$$(\mathcal{A}x)(s,t) = \int_{a(t)}^{s} K_1(s,t,\sigma) \, x(\sigma,t) \, d\sigma + \int_{b(s)}^{t} K_2(s,t,\tau) \, x(s,\tau) \, d\tau.$$

so that Ax = F + Kx

To apply fixed-point theory, we must show that \mathcal{A} is continuous. Let $x, y \in C(\Omega)$ and set $M = \max\{\sup |K_1|, \sup |K_2|\}$. Then

$$\begin{aligned} |(\mathcal{A}x - \mathcal{A}y)(s,t)| &= |(\mathcal{K}x - \mathcal{K}y)(s,t)| \\ &\leq \int_{a(t)}^{s} |K_1(s,t,\sigma)| \left| x(\sigma,t) - y(\sigma,t) \right| d\sigma \\ &+ \int_{b(s)}^{t} |K_2(s,t,\tau)| \left| x(s,\tau) - y(s,\tau) \right| d\tau \\ &\leq M \|x - y\|_{\infty} \left((s - a(t)) + (t - b(s)) \right) \\ &\leq M(S + T) \|x - y\|_{\infty}. \end{aligned}$$

Taking the supremum over $(s,t) \in \Omega$ gives

$$\|\mathcal{A}x - \mathcal{A}y\|_{\infty} \le M(S+T) \|x - y\|_{\infty},$$

so \mathcal{A} is a continuous operator on $C(\Omega)$. Thus, a solution of the integral equation (5.7) corresponds to a fixed point of \mathcal{A} , i.e., $x = \mathcal{A}x$.

The Iterative Sequence: Let $x_0(s,t) \in C(\Omega)$ be an arbitrary continuous function. We generate a sequence $(x_n)_{n=0}^{\infty}$ by the recurrence

$$x_{n+1}(s,t) = (\mathcal{A}x_n)(s,t).$$

To analyze convergence, we write x_n in the series representation form

$$x_n = x_0 + \sum_{k=0}^{n-1} (x_{k+1} - x_k).$$

Defining $u_k = x_{k+1} - x_k$, the convergence of (x_n) is equivalent to the convergence of the series $\sum_{k=0}^{\infty} u_k$. In particular, u_k satisfies the recurrence

$$u_k(s,t) = (\mathcal{K}x_k)(s,t) - (\mathcal{K}x_{k-1})(s,t)$$

$$= \int_{\sigma(t)}^{s} K_1(s,t,\sigma) u_{k-1}(\sigma,t) d\sigma + \int_{h(s)}^{t} K_2(s,t,\tau) u_{k-1}(s,\tau) d\tau.$$

Deriving the Bounding Estimates: We show, by induction, that the following bound holds:

(5.9)
$$|u_k(s,t)| \le L \frac{(2M(s+t))^k}{k!}, \qquad k \ge 0,$$

where $L = ||u_0||_{\infty} = \sup_{(s,t) \in \Omega} |x_1(s,t) - x_0(s,t)|.$

For the base case k=0, the bound $|u_0(s,t)| \leq L$ holds by definition of L. We now prove the inductive step for $k \geq 1$. Assuming the bound holds for k-1, we have:

$$|u_{k}(s,t)| \leq \int_{a(t)}^{s} M|u_{k-1}(\sigma,t)| d\sigma + \int_{b(s)}^{t} M|u_{k-1}(s,\tau)| d\tau$$

$$\leq \int_{0}^{s} ML \frac{(2M(\sigma+t))^{k-1}}{(k-1)!} d\sigma + \int_{0}^{t} ML \frac{(2M(s+\tau))^{k-1}}{(k-1)!} d\tau$$

$$= \frac{2^{k-1}M^{k}L}{k!} \left((s+t)^{k} - t^{k} + (s+t)^{k} - s^{k} \right)$$

$$\leq L \frac{(2M(s+t))^{k}}{k!}.$$

Thus, for all $k \geq 0$, we have the uniform bound

$$||u_k||_{\infty} \le L \frac{(2M(S+T))^k}{k!}.$$

Convergence and Uniqueness: The series $\sum_{k=0}^{\infty} ||u_k||_{\infty}$ is dominated by the convergent series:

$$\sum_{k=0}^{\infty} L \frac{(2M(S+T))^k}{k!} = L \exp(2M(S+T)).$$

By the Weierstrass M-test, $\sum u_k$ converges absolutely and uniformly on Ω . Since $C(\Omega)$ is a complete space, the sequence of partial sums (x_n) converges uniformly to a limit $x \in C(\Omega)$.

To show that x is indeed a solution, we consider the sequence $x_{n+1} = Ax_n$. Since the integral operator A is continuous with respect to the supremum norm, we have:

$$x = \lim_{n \to \infty} x_{n+1} = \lim_{n \to \infty} Ax_n = A\left(\lim_{n \to \infty} x_n\right) = Ax.$$

Thus, x is a fixed point for \mathcal{A} and a solution to the integral equation.

Finally, to prove uniqueness, let x and y be two continuous solutions on Ω , and let v = x - y. Then v must satisfy the homogeneous equation:

$$v(s,t) = \int_{a(t)}^{s} K_1(s,t,\sigma)v(\sigma,t)d\sigma + \int_{b(s)}^{t} K_2(s,t,\tau)v(s,\tau)d\tau,$$

where K_1 and K_2 as in (5.6).

Since $v = \mathcal{K}v$, it implies that $v = \mathcal{K}^k v$ for any integer $k \geq 1$. We then apply the same bounding argument as in (5.9) to the iterates of \mathcal{K} on v to obtain:

$$|v(s,t)| = |(\mathcal{K}^k v)(s,t)| \le V \frac{(2M(s+t))^k}{k!}.$$

Denoting $V = ||v||_{\infty}$ and taking the supremum over $(s,t) \in \Omega$ on both sides gives:

$$||v||_{\infty} \le ||v||_{\infty} \frac{(2M(S+T))^k}{k!}.$$

Let $\Lambda_k = \frac{(2M(S+T))^k}{k!}$. As $k \to \infty$, $\Lambda_k \to 0$. In particular, there is a finite k, sufficiently large, such that $\Lambda_k < \frac{1}{2}$. Therefore, $||v||_{\infty} = 0$ and x = y, which proves that the solution is unique.

Recall the definition of the operator \mathcal{K} given by (5.7). Substituting the explicit expressions of \mathcal{F} , K_1 , K_2 from (5.6) gives the following representation for a continuous function $u \in C(\bar{\Omega})$:

(5.10)
$$(\mathcal{A}u)(s,t) := \frac{1}{2\lambda(s+t)} \Big(\mathcal{G}(s,t) + \int_{(c-t)^+}^s \lambda'(\sigma+t) u(\sigma,t) \, d\sigma + \int_{(c-s)^+}^t \lambda'(s+\tau) u(s,\tau) \, d\tau \Big).$$

where $\mathcal{G}(s,t)$ is the forcing term determined by the weakly compatible boundary data $\{g,h,f,n\}$ (see Definition 5.1).

We also define the normal derivative operator along the Cauchy segment Γ_C by

(5.11)
$$D_n x(\xi) := \lim_{z \to 0^+} \frac{x(s_z, t_z) - x(\xi, c - \xi)}{z}, \ (s_z, t_z) = (\xi + z, c - \xi + z),$$
 for a.e. $\xi \in (0, c)$.

Our goal now is to highlight a key property of the operator \mathcal{A} . The next lemma shows that \mathcal{A} acts as an "improvement" operator for boundary conditions: starting from an input x_0 that satisfies only the Dirichlet data on $\partial\Omega$, the output $x_1 = \mathcal{A}x_0$ automatically also satisfies the normal derivative

condition along the Cauchy segment Γ_C . This shows that enforcement of the derivative condition is built into the structure of \mathcal{A} , rather than requiring successive iterations.

Lemma 5.10. Let $x_0 \in C(\overline{\Omega})$ be a continuous function that satisfies the Dirichlet boundary conditions $\{g, h, f\}$ on $\partial\Omega$. Then the function $x_1 = \mathcal{A}x_0$, defined by (5.10), not only agrees with $\{g, h, f\}$ on $\partial\Omega$ but also satisfies the normal derivative condition

$$D_n x_1(\xi) = n(\xi)$$
 for almost everywhere $\xi \in \Gamma_C$.

Proof. Let $x_0 \in C(\bar{\Omega})$ satisfying the following conditions for $0 \le s \le c$:

$$x_0(s,0) = g(s), \ s \ge c, \ x_0(0,t) = h(t), \ t \ge c, \ x_0(s,c-s) = f(s).$$

We show that $x_1 = \mathcal{A}x_0$ preserves these conditions and, in addition, satisfies the normal derivative condition on Γ_C . It follows directly from the definition of \mathcal{A} that x_1 satisfies the Dirichlet boundary conditions on $\partial\Omega$.

To verify the normal derivative condition on Γ_C , fix $\xi \in (0, c)$. Recalling the definition of the normal derivative operator (5.11), we consider

$$D_n x_1(\xi) = \lim_{z \to 0^+} \frac{x_1(s_z, t_z) - x_1(\xi, c - \xi)}{z},$$

and aim to show that this limit exists and equals $n(\xi)$ for a.e. $\xi \in (0,c)$.

From the definition of the operator \mathcal{A} , and noting that $0 < s_z, t_z < c$, we obtain

$$x_1(s_z, t_z) = \frac{1}{2\lambda(c+2z)} \Big(\mathcal{G}(s_z, t_z) + I_1(z) + I_2(z) \Big),$$

where we have set

$$I_1(z) = \int_{\xi - z}^{\xi + z} \lambda'(\sigma + t_z) \, x_0(\sigma, t_z) \, d\sigma, \quad I_2(z) = \int_{c - \xi - z}^{c - \xi + z} \lambda'(s_z + \tau) \, x_0(s_z, \tau) \, d\tau.$$

Since the integrands of I_1 and I_2 are continuous in z, it follows that $I_1(0) = I_2(0) = 0$. Consequently, substituting into the definition of the normal derivative operator gives

$$D_n x_1(\xi) = \frac{\lambda(c) D_n[\mathcal{G}(s_z, t_z)] - 2\lambda'(c) \mathcal{G}(\xi, c - \xi)}{2\lambda(c)^2} + \frac{1}{2\lambda(c)} \left. \frac{\partial}{\partial z} \left(I_1(z) + I_2(z) \right) \right|_{z=0}.$$

Also, by continuity of the integrands, the last term simplifies to

$$\left. \frac{\partial}{\partial z} \left(I_1(z) + I_2(z) \right) \right|_{z=0} = 4\lambda'(c) x_0(\xi, c - \xi) = 4\lambda'(c) f(\xi).$$

For the term involving \mathcal{G} , note from (5.5) and the fact that $s_z, t_z < c$ that

$$\mathcal{G}(s_z, t_z) = \lambda(c) \Big(f(s_z) + f(c - t_z) + \int_{c - t_z}^{s_z} n(\sigma) \, d\sigma \Big)$$
$$= \lambda(c) \Big(f(\xi + z) + f(\xi - z) + \int_{c - z}^{\xi + z} n(\sigma) \, d\sigma \Big).$$

By the Lebesgue differentiation theorem, and since $n \in L^1(\Gamma_C)$, the following holds for almost every $\xi \in (0, c)$.

$$D_n[\mathcal{G}(\xi)] = \lim_{z \to 0^+} \frac{\lambda(c) (f(\xi + z) + f(\xi - z) - 2f(\xi))}{z} + 2\lambda(c)n(\xi).$$

Combining this with the previous computation, we obtain

$$D_n x_1(\xi) = \frac{1}{2\lambda(c)} \left(\lim_{z \to 0^+} \frac{\lambda(c) (f(\xi + z) + f(\xi - z) - 2f(\xi))}{z} \right)$$

$$+2\lambda(c)n(\xi)-4\lambda'(c)f(\xi)+4\lambda'(c)f(\xi)$$
.

The last two terms cancel, leaving

$$D_n x_1(\xi) = \lim_{z \to 0^+} \frac{f(\xi + z) + f(\xi - z) - 2f(\xi)}{2z} + n(\xi),$$

which holds for almost every $\xi \in (0, c)$.

At any point ξ where $f'(\xi)$ exists, the limit term can be rewritten as

$$\lim_{z \to 0^+} \frac{f(\xi + z) + f(\xi - z) - 2f(\xi)}{2z} = \frac{1}{2} \lim_{z \to 0^+} \frac{f(\xi + z) - f(\xi)}{z} + \frac{1}{2} \lim_{z \to 0^+} \frac{f(\xi - z) - f(\xi)}{z}.$$

Both limits exist and equal $f'(\xi)$, so the expression:

$$\lim_{z \to 0^+} \frac{f(\xi + z) + f(\xi - z) - 2f(\xi)}{2z} = 0,$$

leaving behind $D_n x_1(\xi) = n(\xi)$.

The improvement property of \mathcal{A} developed in Lemma 5.10 plays a central role in the analysis. It ensures that the boundary conditions are precisely encoded in the operator framework. We now turn to the main proposition of this section, which establishes both the existence of a unique solution and its attainment of the full Cauchy–Goursat boundary conditions.

Proposition 5.11. Let the Cauchy–Goursat data $\{g, h, f, n\}$ be weakly compatible. Then the associated Volterra integral equation

$$x(s,t) = \mathcal{F}(s,t) + \int_{(c-t)^+}^{s} K_1(s,t,\sigma) \, x(\sigma,t) \, d\sigma + \int_{(c-s)^+}^{t} K_2(s,t,\tau) \, x(s,\tau) \, d\tau.$$

possesses a unique continuous solution $x \in C(\overline{\Omega})$. Moreover, the solution attains the prescribed Cauchy–Goursat boundary conditions $\{g,h,f,n\}$.

Proof. The proof proceeds in two main steps: establishing the existence of a unique solution and demonstrating that this solution attains the boundary conditions.

Existence and uniqueness. Given weakly compatible data, the forcing term which is defined by

$$\mathcal{F}(s,t) = \frac{\mathcal{G}(s,t)}{2\lambda(s+t)},$$

is continuous on any compact subdomain of the form

$$\bar{\Omega} \cap [0, S] \times [0, T] = \{(s, t) \mid 0 \le s \le S, \ 0 \le t \le T, \ s + t \ge c > 0\}.$$

The kernels K_1 and K_2 are likewise continuous on their respective domains.

By Theorem. 5.8, there exists a unique continuous solution $x_{S,T}$ on each rectangle $[0, S] \times [0, T]$ intersected with $\bar{\Omega}$. Exhausting $\bar{\Omega}$ by such rectangles establishes the existence of a unique continuous solution $x \in C(\bar{\Omega})$. This solution is the fixed point of the operator A, i.e., x = Ax.

Attainment of boundary conditions. To show that the unique solution x satisfies the prescribed boundary conditions, we examine the sequence of successive approximations used to construct it.

We begin by constructing a suitable initial guess x_0 . By weak compatibility, there exists a continuous boundary function on $\partial\Omega$ that agrees with the Dirichlet data $\{g, h, f\}$. By the Tietze extension theorem, this extends to a continuous function $x_0 \in C(\bar{\Omega})$ agreeing with $\{g, h, f\}$ on $\partial\Omega$.

Next, define the sequence $x_k = \mathcal{A}x_{k-1}$ for $k \geq 1$. By Theorem 5.8, $x_k \to x$ uniformly on compact subdomains. Moreover, since x_0 agrees with $\{g, h, f\}$ on $\partial\Omega$, Lemma 5.10 and induction guarantee that every iterate x_k also satisfies the Dirichlet conditions.

Passing to the limit, we conclude that x itself satisfies the Dirichlet conditions. For instance, at any boundary point (s, 0) with $s \ge c$,

$$x(s,0) = \lim_{k \to \infty} x_k(s,0) = \lim_{k \to \infty} g(s) = g(s),$$

and the same holds for Γ_2 and Γ_C .

Finally, since the unique solution x satisfies the Dirichlet conditions, Lemma 5.10 applies to x itself. The lemma asserts that Ax satisfies the normal derivative condition. But x is the unique fixed point of A, so Ax = x. Hence,

$$D_n x(\xi) = n(\xi)$$
 for a.e. $\xi \in [0, c]$.

This completes the proof that the unique solution to the Volterra equation attains all prescribed Cauchy–Goursat boundary conditions. \Box

6. SINGULARITIES AND THEIR RESOLUTION

A central theme in the theory of PDEs is that solution regularity depends not only on the smoothness of the data but also on the geometry of the problem. Our analysis in the hodograph plane faces two distinct challenges, which this section addresses in turn. The first is the existence of a well-posed solution x(s,t), which is complicated by the *corner singularities* inherent to the Cauchy–Goursat geometry. They arise at the transition from non-characteristic (Cauchy) to characteristic (Goursat) boundaries and

are present even for solutions that are smooth in the interior. The second challenge is the physical interpretation of a solution once it is found. The inverse map from the hodograph plane back to physical space can fail, creating fold singularities [4] where the solution x(s,t) no longer represents a valid, non-degenerate surface w(x,y).

Our approach is to first build a framework to resolve the corner singularity and construct a mathematical solution, and then to investigate the conditions under which that solution is free of folds. We begin by using an exact "arcsine" solution as a key example to demonstrate how singular boundary data is naturally generated. We then perform a local asymptotic analysis to reveal the universal square-root cusp behavior near the characteristic boundaries. This motivates the construction of a parametrix that captures this singular structure, reducing the problem to finding a more regular corrector function. Finally, having established a robust method for finding solutions in the hodograph plane, we analyze the inverse problem and the formation of fold singularities.

Example 6.1 (The "arcsine" solution). From Section 4, we know that $\lambda(u) = u$ admits a product solution with

$$u = Ae^{-y}$$
, $w(x, y) = Ae^{-y}\cos(x)$, and $p = w_x = -Ae^{-y}\sin(x)$.

We "solve" for x in terms of u and p to get

(6.1)
$$x_a(s,t) = \arcsin\left(-\frac{p}{u}\right) = \arcsin\left(\frac{t-s}{t+s}\right),$$

and consider the governing equation

$$(6.2) 2(s+t)x_{st} + x_s + x_t = 0.$$

A direct calculation verifies that the function $x_a(s,t)$ is a solution to the above equation for s > 0, t > 0. This solution is analytic in the open first quadrant.

Let us examine the boundary data it induces on the following domain $\Omega = \{(s,t) \in \mathbb{R}^2 \mid s > 0, t > 0, s+t > c\}$, for some c > 0.

• Goursat Data on Γ_1 and Γ_2 :

For $s \ge c$, the boundary value on Γ_1 is $g(s) = x_a(s,0) = \arcsin(-1) = -\frac{\pi}{2}$.

For $t \geq c$, the boundary value on Γ_2 is $h(t) = x_a(0,t) = \arcsin(1) = \frac{\pi}{2}$.

• Cauchy Data on Γ_C : For $0 \le s \le c$, we have t = c - s. The Dirichlet data is

$$f(s) = x_a(s, c - s) = \arcsin\left(\frac{c - s - s}{c - s + s}\right) = \arcsin\left(\frac{c - 2s}{c}\right).$$

The associated normal derivative on Γ_C is then computed as:

$$n(s) = (\partial_s + \partial_t)x_a(s,t)\big|_{t=c-s} = \frac{2s-c}{c\sqrt{s(c-s)}}.$$

This example illustrates that the boundary data set $\{g, h, f, n\}$ generated by the smooth interior solution x_a is appropriate for our weak compatibility of boundary data, as seen in Definition 5.1. Namely,

(1) **Continuity of Dirichlet data.** The boundary data is continuous at the corners:

$$(c,0): g(c) = -\frac{\pi}{2}, \quad f(c) = \arcsin\left(\frac{c-2c}{c}\right) = -\frac{\pi}{2}, \quad \text{so } g(c) = f(c).$$

$$(0,c): h(c) = \frac{\pi}{2}, \qquad f(0) = \arcsin(\frac{c}{c}) = \frac{\pi}{2}, \qquad \text{so } h(c) = f(0).$$

- (2) **Absolute continuity of** f. The tangential derivative is given by $f'(s) = -1/\sqrt{s(c-s)}$. While this derivative is singular at s = 0 and s = c, it is integrable over [0, c]. Thus, f is absolutely continuous and $f' \in L^1(\Gamma_C)$.
- (3) Integrability of n. The normal derivative n(s) has inverse-square-root singularities at the endpoints. These singularities are integrable, and thus $n \in L^1(\Gamma_C)$.

The crucial point is that, although the data satisfy all the weak compatibility requirements, the normal derivative n(s) is manifestly unbounded as $s \to 0^+$ and $s \to c^-$. Hence this data set cannot be the trace of any $C^1(\bar{\Omega})$ function. This example illustrates the necessity of weak compatibility, as smooth interior solutions may still generate singular boundary traces at the corners.

6.1. Asymptotic Analysis near a Goursat Boundary. To better understand the solution's structure near a characteristic (Goursat) boundary, we carry out a local analysis of the behavior as $s \to 0^+$ with t > c. The same reasoning applies in both the finite and infinite cylinder cases. Motivated by the arcsine solution (6.1), which exhibits a square-root singularity in its gradient, we posit the ansatz

$$x(s,t) = h(t) + A(t)\sqrt{s} + o(\sqrt{s}), \quad s \to 0^+,$$

where x(0,t) = h(t) is the prescribed Goursat data on that boundary. The relevant partial derivatives become:

$$x_s(s,t) = \frac{1}{2}A(t) s^{-1/2} + o\left(s^{-1/2}\right),$$

$$x_t(s,t) = h'(t) + A'(t)\sqrt{s} + o\left(\sqrt{s}\right),\,$$

$$x_{st}(s,t) = \frac{1}{2}A'(t) s^{-1/2} + o\left(s^{-1/2}\right).$$

Since s is small, we expand the coefficients $\lambda(s+t)$ and $\lambda'(s+t)$ in a Taylor series around t:

$$\lambda(s+t) = \lambda(t) + \lambda'(t)s + O(s^2), \quad \lambda'(s+t) = \lambda'(t) + \lambda''(t)s + O(s^2).$$

Substituting these relations into the governing partial differential equation $2\lambda(s+t)x_{st} + \lambda'(s+t)(x_s+x_t) = 0$, we obtain that the following expression

must vanish:

$$2(\lambda(t) + O(s)) \left(\frac{1}{2} A'(t) s^{-1/2} + \dots \right) + (\lambda'(t) + O(s)) \left(\frac{1}{2} A(t) s^{-1/2} + h'(t) + \dots \right).$$

To find the condition for this equation to hold, we collect the coefficients of the most singular term, $s^{-1/2}$:

$$2\lambda(t)\left(\frac{1}{2}A'(t)\right) + \lambda'(t)\left(\frac{1}{2}A(t)\right) = 0.$$

Balancing the leading-order terms gives a first-order ordinary differential equation for the amplitude function A(t):

$$\lambda(t)A'(t) + \frac{1}{2}\lambda'(t)A(t) = 0$$

and the solution is given by

(6.3)
$$A(t) = M[\lambda(t)]^{-1/2},$$

where M is a constant of integration.

6.2. The Parametrix and Corrector Solutions. The previous calculation shows that, for a solution to exhibit the square-root cusp behavior near the boundary s=0, the amplitude A(t) cannot be arbitrary but scale like $\lambda(t)^{-1/2}$. This motivates a natural deformation of the arcsine solution from Example 6.1, namely

$$x_p(s,t) = \arcsin\left(\frac{\lambda(t) - \lambda(s)}{\lambda(t) + \lambda(s)}\right).$$

Expanding this expression for small s yields

$$\arcsin\!\left(\frac{\lambda(t)-\lambda(s)}{\lambda(t)+\lambda(s)}\right) \approx \arcsin\!\left(1-\frac{2\lambda(s)}{\lambda(t)}\right) \approx \frac{\pi}{2} - 2\sqrt{\frac{\lambda(s)}{\lambda(t)}} \approx \frac{\pi}{2} - \frac{M}{\sqrt{\lambda(t)}}\sqrt{s},$$

for some constant M, consistent with the square-root asymptotics obtained in (6.3).

We think of x_p as a "parametrix," i.e., an approximate solution of the PDE that satisfies the Goursat boundary conditions $x(s,0) = x_+$ and $x(0,t) = x_-$, which are discontinuous at the origin, while also capturing the leading-order singular behavior of x. While the term parametrix typically denotes an approximate inverse operator [16], our usage follows its strategic purpose of providing an approximate solution that captures the principal singular behavior, thereby regularizing the problem for the remainder of the solution, the *corrector term*.

The governing PDE for x is given by L[x] = 0, where the linear operator is defined in (3.6). Let us now define the residual operator by

$$\mathcal{H}(s,t) := L[x_n],$$

that captures the result of applying the PDE operator to the parametrix. In general, this residual is not zero. We therefore introduce the *corrector* solution $x_{\text{corr}}(s,t)$, chosen such that

$$x_{\text{base}} = x_p + x_{\text{corr}}$$

satisfies both the PDE $L[x_{\text{base}}] = 0$ and the appropriate boundary conditions.

Since x_p was constructed to satisfy the original Goursat data, the corrector x_{corr} necessarily satisfies homogeneous Goursat boundary conditions. Thus, the problem for x_{corr} reduces to solving a Goursat problem with homogeneous boundary data and forcing term $-L[x_p] = -\mathcal{H}$. This strategy is effective only if the residual \mathcal{H} is smoother than the singular parametrix x_p .

For the analysis that follows, we fix the domains for S > 0, T > 0 as

(6.4)
$$R := [0, S] \times [0, T], \quad R_0 := R \setminus \{\mathbf{0}\}.$$

We first establish the regularity of the residual \mathcal{H} , which will play a central role in the construction of the corrector.

Lemma 6.2 (Regularity of the Residual). Suppose $\lambda(u)$ is smooth for u > 0 with $\lambda'(0) > 0$. Then the residual $\mathcal{H}(s,t) = L[x_p]$ is smooth on the domain $(0,S) \times (0,T)$. Moreover, there exists a constant $M_H > 0$ such that, for all $(s,t) \in R_0$, we have the bound

$$|\mathcal{H}(s,t)| \le M_H \frac{\sqrt{st}}{s+t}.$$

Proof. A direct computation of $\mathcal{H}(s,t) = L[x_p]$ gives

$$\begin{split} \mathcal{H}(s,t) = & \frac{1}{\sqrt{\lambda(s)\lambda(t)} \left(\lambda(s) + \lambda(t)\right)^2} \bigg[-\lambda(s)^2 \lambda'(t) \lambda'(s+t) \\ & + \lambda(t)\lambda'(s) \big(-\lambda(s+t)\lambda'(t) + \lambda(t)\lambda'(s+t) \big) \\ & + \lambda(s) \big(\lambda(s+t)\lambda'(s)\lambda'(t) + \lambda(t)(\lambda'(s) - \lambda'(t))\lambda'(s+t) \big) \bigg]. \end{split}$$

The denominator is smooth and strictly positive for s > 0, t > 0, hence \mathcal{H} is smooth on $(0, S) \times (0, T)$. To establish the bound on R_0 , it remains to estimate the behavior of $\mathcal{H}(s,t)$ as (s,t) approaches the boundary ∂R , in particular as $s \to 0$, $t \to 0$, or $s + t \to 0$.

A direct computation, under the assumption $\lambda'(0) > 0$, gives

$$\lim_{t>0, s\to 0^+} \frac{\mathcal{H}(s,t)}{\sqrt{st}} = \frac{\sqrt{\lambda'(0)} \left(\lambda(t)\lambda''(t) - 2\lambda'(t)^2 + 2\lambda'(0)\lambda'(t)\right)}{\lambda(t)^{3/2}} + O(s),$$

with an analogous expression obtained by interchanging s and t for the limit s > 0, $t \to 0$. This quantity is continuous in t, except possibly at t = 0. To

analyze the behavior at this endpoint, we examine the limit:

$$\lim_{t \to 0^{+}} \lim_{s \to 0^{+}} \frac{(s+t) \mathcal{H}(s,t)}{\sqrt{st}}$$

$$= \lim_{t \to 0^{+}} t \frac{\sqrt{\lambda'(0)} \left(\lambda(t)\lambda''(t) - 2\lambda'(t)^{2} + 2\lambda'(0)\lambda'(t)\right)}{\lambda(t)^{3/2}} + O(s)$$

$$= -\lambda''(0).$$

Because x_p is antisymmetric while the operator L is symmetric under the interchange $s \leftrightarrow t$, we obtain

$$\lim_{t \to 0^+} \lim_{s \to 0^+} \frac{(s+t)\mathcal{H}(s,t)}{\sqrt{st}} = \lambda''(0).$$

Thus the limit depends on the direction of approach to the origin. To analyze the behavior as $s, t \to 0$ along different paths, we introduce the rescaled variables $s = \alpha u$ and $t = \beta u$ where u = s + t and we have $0 \le \alpha, \beta$ with $\alpha + \beta = 1$. With this change of variables, and using the local expansion

$$\lambda(u) = u + \frac{1}{2}\lambda''(0)u^2 + O(u^3)$$
 as $u \to 0$,

we compute

$$\lim_{u \to 0, s = \alpha u, t = \beta u} \frac{(s+t)\mathcal{H}(s,t)}{\sqrt{st}} = (\alpha - \beta) \lambda''(0).$$

Since $|\alpha - \beta| \leq 1$ and $2\sqrt{st} \leq s + t$, it follows that $\mathcal{H}(s,t)$ is a bounded continuous function on R_0 . In general, \mathcal{H} does not extend continuously to R, but it can be extended as a bounded measurable function by, for instance, defining $\mathcal{H}(\mathbf{0}) = 0$.

We now introduce a function space that will facilitate the analysis of the corrector problem.

Definition 6.3 (Lipschitz functions vanishing on the axes). We define the Banach space

$$\mathrm{Lip}_0(R) := \Big\{ \, x \in C(R) \, \, \Big| \, \, x(s,0) = x(0,t) = 0 \, \, \text{for} \, \, 0 \leq s \leq S, \, \, 0 \leq t \leq T \, \Big\},$$

equipped with the Lipschitz norm

$$||x||_{\text{Lip}} := \sup_{p_1 \neq p_2 \in R} \frac{|x(p_1) - x(p_2)|}{|p_1 - p_2|} < \infty.$$

Any function $x \in \text{Lip}_0(R)$ satisfies the pointwise bound

$$|x(s,t)| \leq \|x\|_{\mathrm{Lip}} \min(s,t) \leq \|x\|_{\mathrm{Lip}} (s+t).$$

Within this setup, the residual \mathcal{H} gives rise to an integrated quantity, which we now show belongs to $\operatorname{Lip}_0(R)$.

Lemma 6.4 (Regularity of the Integrated Forcing Term). Let f(s,t) denote the forcing term for the integral equation for the corrector, defined by

$$f(s,t) = -\frac{1}{2\lambda(s+t)} \int_0^s \int_0^t \mathcal{H}(\sigma,\tau) \, d\sigma \, d\tau.$$

Then $f \in \text{Lip}_0(R)$. That is, f is Lipschitz continuous on R and vanishes on the coordinate axes s = 0 and t = 0.

Proof. Consider the integrated residual,

$$I(s,t) := \int_0^s \int_0^t \mathcal{H}(\sigma,\tau) \, d\sigma \, d\tau.$$

From the preceding lemma, the residual \mathcal{H} is a bounded measurable function on R, with $|\mathcal{H}| \leq M_H$ for some constant $M_H > 0$. It follows immediately that I(s,0) = I(0,t) = 0, and therefore f(s,0) = f(0,t) = 0 for all s,t > 0.

We begin by obtaining a pointwise bound for f. Using the bound on \mathcal{H} , we estimate the integral as

$$|I(s,t)| \leq M_H st.$$

For s+t>0, we have $\lambda(s+t)>0$. Near the origin, $\lambda(u)\approx \lambda'(0)u$, so for some constant $C_1>0$, we have $\lambda(s+t)\geq C_1(s+t)$ on R. This gives the bound:

$$|f(s,t)| = \frac{|I(s,t)|}{2\lambda(s+t)} \le \frac{M_H st}{2C_1(s+t)}.$$

By the AM-GM inequality, since $2\sqrt{st} \le s + t$, it follows that $\frac{st}{s+t} \le \frac{\sqrt{st}}{2}$. This shows that $|f(s,t)| \le C_2\sqrt{st}$ for some constant C_2 , verifying that f is continuous up to the origin with $f(\mathbf{0}) = 0$.

To prove Lipschitz continuity, it is enough to show that the partial derivatives of f are bounded. These are given by

$$I_s(s,t) = \int_0^t \mathcal{H}(s,\tau) d\tau, \quad I_t(s,t) = \int_0^s \mathcal{H}(\sigma,t) d\sigma,$$

and are bounded by $|I_s(s,t)| \leq M_H t$ and $|I_t(s,t)| \leq M_H s$. By the quotient rule, the partial derivative of f with respect to s is

$$f_s(s,t) = -\frac{I_s(s,t)\,\lambda(s+t) - I(s,t)\,\lambda'(s+t)}{2\lambda(s+t)^2}.$$

Using our bounds on I, I_s , and the linear behavior of λ and λ' near the origin, the numerator is bounded by $O(t(s+t)+st)=O(st+t^2)$, while the denominator is $O((s+t)^2)$. The quotient is therefore bounded for small s and t. Away from the origin, all terms are continuous and bounded on the compact domain R.

A similar argument applies to f_t . Thus f is Lipschitz continuous on R. \square

We now prove the existence of the corrector solution, showing that it is more regular than the parametrix x_p , which is discontinuous at **0**.

6.3. Existence and Uniqueness for the Corrector. The existence and uniqueness of the corrector can be expressed through an associated Volterra integral equation. Specifically, we consider

(6.5)
$$x(s,t) = f(s,t) + \int_0^s K_1(s,t,\sigma) x(\sigma,t) d\sigma + \int_0^t K_2(s,t,\tau) x(s,\tau) d\tau,$$

for an unknown function $x \in C_0(R)$, where $R = [0, S] \times [0, T]$ and $C_0(R)$ denotes the Banach space of continuous functions on R that vanish on the axes s = 0 and t = 0.

The kernels are defined for s + t > 0 by

$$K_1(s,t,\sigma) = \frac{\lambda'(\sigma+t)}{2\lambda(s+t)}, \qquad K_2(s,t,\tau) = \frac{\lambda'(s+\tau)}{2\lambda(s+t)}.$$

Theorem 6.5. Let the kernels K_1 and K_2 be defined as above. Suppose λ satisfies:

- (1) $\lambda(0) = 0$;
- (2) λ is continuously differentiable on (0, S+T), with one-sided derivatives at the endpoints, and $\lambda'(u) > 0$ for all $u \in [0, S+T]$.

Then, for any $f \in C_0(R)$, the Volterra equation (6.5) admits a unique solution $x \in C_0(R)$.

Proof. The proof uses the Banach Fixed-Point Theorem. We rewrite (6.5) in the form

$$x = \mathcal{A}(x), \quad \mathcal{A}(x) := f + \mathcal{K}x,$$

where K is the linear integral operator defined in (5.8) by the kernels K_1 and K_2 .

Preservation of boundary conditions. The operator \mathcal{A} preserves the property of vanishing on the axes. Indeed, if $x \in C_0(R)$ satisfies x(s,0) = 0 and x(0,t) = 0, then

$$(\mathcal{A}x)(s,0) = f(s,0) + \int_0^s K_1(s,0,\sigma) x(\sigma,0) d\sigma = 0,$$

$$(\mathcal{A}x)(0,t) = f(0,t) + \int_0^t K_2(0,t,\tau) \, x(0,\tau) \, d\tau = 0.$$

Thus \mathcal{A} maps $C_0(R)$ into itself. Moreover, away from the origin $\mathbf{0}$, the kernels K_1 and K_2 are continuous in (s,t), so \mathcal{A} preserves continuity on R.

Behavior at the origin. The kernels are well defined for s + t > 0, but at the origin the denominator $\lambda(s+t)$ vanishes. We set $(\mathcal{A}u)(\mathbf{0}) = 0$, which yields continuity, as the following limit evaluates to zero:

$$\lim_{(s,t)\to\mathbf{0}} x(s,t) = f(\mathbf{0}) + \lim_{s\to 0} \frac{1}{2\lambda(s)} \int_0^s \lambda'(s+\sigma) \, x(\sigma,0) \, d\sigma$$
$$+ \lim_{t\to 0} \frac{1}{2\lambda(t)} \int_0^t \lambda'(s+\tau) \, x(0,\tau) \, d\tau.$$

Contraction property. We now estimate the operator norm on $C_0(R)$ with the supremum norm $\|\cdot\|_{\infty}$:

(6.6)
$$\|\mathcal{K}\|_{\infty} = \sup_{(s,t)\in R} \left\{ \int_0^s |K_1(s,t,\sigma)| \, d\sigma + \int_0^t |K_2(s,t,\tau)| \, d\tau \right\}.$$

From the hypothesis, the function

(6.7)
$$g(u) := \frac{\lambda(u)}{u}, \quad u > 0,$$

can be extended continuously to [0, S + T] by $g(0) := \lambda'(0)$. Since g is continuous on this compact interval, the Extreme Value Theorem guarantees that the following are attained:

$$m_0 := \inf_{u \in [0, S+T]} g(u), \qquad M := \sup_{u \in [0, S+T]} g(u).$$

By the Mean Value Theorem, for every u > 0 there exists $\xi \in (0, u)$ such that $g(u) = \lambda'(\xi)$, and thus g(u) > 0. At u = 0 we have $g(0) = \lambda'(0) > 0$. Consequently, $m_0 > 0$. In addition, since g is continuous on a compact set, we also have $M < \infty$.

Because $\lambda'(u) > 0$ and $\lambda(u) = ug(u) > 0$ for u > 0, the kernels are nonnegative. Hence the operator norm (6.6) becomes

$$\|\mathcal{K}\|_{\infty} = \sup_{(s,t)\in R_0} \left\{ \int_0^s K_1(s,t,\sigma) \, d\sigma + \int_0^t K_2(s,t,\tau) \, d\tau \right\}.$$

Evaluating the integrals yields

$$\int_0^s K_1(s,t,\sigma) d\sigma = \frac{\lambda(s+t) - \lambda(t)}{2\lambda(s+t)},$$

$$\int_0^t K_2(s,t,\tau) d\tau = \frac{\lambda(s+t) - \lambda(s)}{2\lambda(s+t)},$$

and their sum becomes

$$1 - \frac{\lambda(s) + \lambda(t)}{2\lambda(s+t)}.$$

In terms of g given by (6.7), we have

$$\frac{\lambda(s)+\lambda(t)}{2\lambda(s+t)} = \frac{sg(s)+tg(t)}{2(s+t)g(s+t)} \ \geq \ \frac{m_0}{2M}.$$

Thus,

$$\int_0^s K_1 \, d\sigma + \int_0^t K_2 \, d\tau \, \leq \, 1 - \frac{m_0}{2M},$$

for all $(s,t) \in R$. Hence

$$||K||_{\infty} \le 1 - \frac{m_0}{2M} < 1.$$

Therefore K is a contraction on $C_0(R)$. By the Banach Fixed-Point Theorem, A has a unique fixed point, which is the unique solution to (6.5). Since $x \in C_0(R)$, this solution vanishes on the coordinate axes as well.

6.4. The Inverse Problem and Fold Singularities. The transformation from the physical coordinates (x, y) to the characteristic coordinates (s, t) is a powerful tool because it converts the nonlinear Monge–Ampère equation into an equivalent linear formulation. In particular, every "partially convex" classical solution w(x, y) (i.e., one for which w_{xx} is everywhere positive or everywhere negative) corresponds to a solution x(s, t) of the linear integral equation analyzed above.

This raises a natural question: can we always reverse the process? That is, can any solution x(s,t) of the integral equation be transformed back to recover a classical solution w(x,y)? In general the answer is no: the inversion of the hodograph transformation is not always possible. The following example shows concretely how this failure can occur.

Example 6.6 (Birth of a Singularity from Weakly Compatible Data). Consider the case $\lambda(u) = u$, for which the associated linear PDE is the Euler–Poisson–Darboux equation, $u(x_{uu} - x_{pp}) + x_u = 0$. An exact polynomial solution for this is

$$x_{\text{poly}}(u, p) = -\frac{5\pi}{26} \left[(3u^4 - 12u^2 + 10)p + 8(u^2 - 1)p^3 + \frac{8}{5}p^5 \right],$$

with derivative with respect to p given by

$$(x_{\text{poly}})_p(u,p) = -\frac{5\pi}{26} \left[(3u^4 - 12u^2 + 10) + 24(u^2 - 1)p^2 + 8p^4 \right].$$

Consider now the domain $\Omega_1 = \{(s,t) \mid s,t \geq 0, s+t \geq 1\}$. We pose a Cauchy–Goursat problem with the boundary data defined as follows.

• Cauchy Data on u = 1: For $p \in [-1, 1]$, we prescribe boundary data that agree with those of the exact polynomial solution

Dirichlet data:
$$x(1,p) = -\frac{\pi}{26}(5p + 8p^5),$$

Normal derivative:
$$x_u(1, p) = -\frac{10\pi}{13} p(4p^2 - 3)$$
.

The concavity condition is then satisfied along the Cauchy boundary u=1, since $(x_{\text{poly}})_p(1,p)=-\frac{5\pi}{26}(1+8p^4)<0$ for all $p\in[-1,1]$.

• Goursat Data on $p = \pm u$: For u > 1, we prescribe constant Goursat data, taking the values from the corners of the Cauchy segment:

$$x(u, u) = x_{\text{poly}}(1, 1) = -\frac{5\pi}{26} \left(1 + \frac{8}{5}\right) = -\frac{\pi}{2},$$

$$x(u, -u) = x_{\text{poly}}(1, -1) = \frac{5\pi}{26} \left(1 + \frac{8}{5}\right) = \frac{\pi}{2}.$$

This defines a well-posed problem. At the corners where the boundary type changes, for instance, at (u,p)=(1,1), the Dirichlet data is continuous by construction. The derivatives, however, do not match: along the Goursat boundary p=u the tangential derivative vanishes, whereas along the Cauchy segment u=1 we have $(x_{\text{poly}})_u(1,1)+(x_{\text{poly}})_p(1,1)=-\frac{5\pi}{2}$.

Thus, the data is not C^1 -compatible. It is, however, weakly compatible, fitting precisely into the framework we have developed for such solutions. The unique solution within the domain of dependence of the Cauchy data,

the "central diamond" $|u-1|+|p-1| \leq 2$, is given by the polynomial $x(u,p) = x_{\text{poly}}(u,p)$.

We now demonstrate the "birth" of a singularity within this region. At the interior point $(u^*, p^*) = (\frac{3}{2}, 0)$, we find $x_p(u^*, p^*) = \frac{145\pi}{416}$. Initially, $x_p < 0$ everywhere on the boundary at u = 1, but inside the domain it evolves to $x_p > 0$ at this point. Thus, a fold singularity [4] must form since x_p crosses zero, appearing spontaneously ("out of nowhere") from otherwise regular data. Outside the central diamond the polynomial no longer represents the solution, but the solution itself remains continuous, as guaranteed by Theorem 5.8.

7. Energy Estimates and Stability for the Cauchy–Goursat Problem

A central tool for analyzing hyperbolic problems is the use of energy identities [12], which provide quantitative control of solutions even when singularities are present. In this section, we derive an energy estimate for the Cauchy–Goursat problem in characteristic variables. The resulting identity balances the growth of the solution against dissipation and forcing, and yields stability bounds that are uniform with respect to the geometry of the domain. Beyond clarifying the behavior of the linearized model, these estimates also feed directly into the analysis of the hyperbolic Monge–Ampère equation on the cylinder, where they play a key role in establishing stability under perturbations of the coefficient function.

7.1. **Energy Identity and Estimates.** Let's start by considering the non-homogeneous problem

(7.1)
$$2\lambda(s+t)x_{st} + \lambda'(s+t)(x_s + x_t) = g(s,t)$$

on the domain $\Omega = \{(s,t) \mid s,t \geq 0, s+t \geq c\}$, with $\lambda \in C^1$, $\lambda > 0$, and $\lambda' > 0$ for s+t > 0. The solution x(s,t) is assumed to satisfy the homogeneous Goursat boundary conditions

$$x(s,0) = 0$$
 for $s \ge c$, $x(0,t) = 0$ for $t \ge c$.

Proposition 7.1. Let x(s,t) be a C^2 solution of the problem above. Define the energy along the line $\Gamma_u: s+t=u$ by

(7.2)
$$E(u) = \int_0^u \lambda(u) \Big((x_s(s, u - s))^2 + (x_t(s, u - s))^2 \Big) ds.$$

Then for any u > c, the solution satisfies the energy identity

(7.3)
$$E(u) = E(c) + \int_{c}^{u} \int_{0}^{v} \left(g(x_s + x_t) - 2\lambda'(v) x_s x_t \right) ds \, dv,$$

where the integrands on the right are evaluated at (s, v - s).

Proof. The proof proceeds by first deriving a local conservation law and then integrating it over the domain.

Step 1: Derivation of the Conservation Law. We multiply (7.1) by $(x_s + x_t)$ to get:

$$2\lambda x_{st}(x_s + x_t) + \lambda'(x_s + x_t)^2 = g(x_s + x_t),$$

which can be rewritten as

$$\frac{\partial}{\partial t}(\lambda x_s^2) + \frac{\partial}{\partial s}(\lambda x_t^2) - \lambda'(x_s^2 + x_t^2) + \lambda'(x_s + x_t)^2 = g(x_s + x_t).$$

Expanding the squared term and simplifying, we arrive at the conservation law:

(7.4)
$$\frac{\partial}{\partial t} (\lambda x_s^2) + \frac{\partial}{\partial s} (\lambda x_t^2) + 2\lambda' x_s x_t = g(x_s + x_t).$$

Step 2: Integration over the Domain. We now integrate (7.4) over the domain $D_u = \{(s',t') \mid c \leq s' + t' \leq u, s' \geq 0, t' \geq 0\}$. By Green's theorem, the divergence term contributes boundary integrals. The characteristic sides vanish due to homogeneous Goursat conditions, while the lines s + t = u and s + t = c contribute E(u) and -E(c), respectively. Thus, the integral of the divergence part is E(u) - E(c).

Equating the integrated parts gives

$$E(u) - E(c) + \iint_{D_u} 2\lambda' x_s x_t \, ds' dt' = \iint_{D_u} g(x_s + x_t) \, ds' dt'.$$

Rearranging and writing the integrals in iterated form yields the final identity (7.3).

Corollary 7.2. [Energy Estimate for the Solution] Let x be a solution to the inhomogeneous problem on the domain

$$\Omega_u = \{ (s, \zeta - s) \mid c \le \zeta \le u, \ 0 \le s \le \zeta \}.$$

If $\lambda'(\zeta) > 0$ for all $\zeta \geq c$, then the energy satisfies the bound

(7.5)
$$E(u) \le \frac{\lambda(u) \exp(u - c)}{\lambda(c)} \left(E(c) + \frac{1}{2} \|g\|_{L^2(\Omega_u)}^2 \right), \quad u > c.$$

where

$$||g||_{L^2(\Omega_u)}^2 = \int_c^u \int_0^\zeta g(s, \zeta - s)^2 \, ds \, d\zeta.$$

Proof. We start from the energy identity (7.3). We bound the terms on the right-hand side using the Cauchy–Schwarz and Young inequalities:

$$|g(x_s + x_t)| \le \frac{1}{2}g^2 + \frac{1}{2}(x_s + x_t)^2 \le \frac{1}{2}g^2 + x_s^2 + x_t^2,$$

$$|-2\lambda' x_s x_t| \le \lambda'(x_s^2 + x_t^2).$$

Substituting these inequalities into (7.3) yields

$$E(u) \le E(c) + \int_{c}^{u} \int_{0}^{v} \left(\frac{1}{2}g^{2} + x_{s}^{2} + x_{t}^{2}\right) ds dv + \int_{c}^{u} \int_{0}^{v} \lambda'(v)(x_{s}^{2} + x_{t}^{2}) ds dv$$

$$\le E(c) + \frac{1}{2} \|g\|_{L^{2}(\Omega_{u})}^{2} + \int_{c}^{u} \int_{0}^{v} (1 + \lambda'(v))(x_{s}^{2} + x_{t}^{2}) ds dv.$$

Using E(v) given by (7.2) we can write the last term as:

$$E(u) \le E(c) + \frac{1}{2} \|g\|_{L^2(\Omega_u)}^2 + \int_c^u \frac{1 + \lambda'(v)}{\lambda(v)} E(v) dv.$$

Finally, applying Gronwall's lemma yields the bound (7.5).

7.2. Stability under Perturbations of the Curvature Function. We next analyze the stability of the solution x with respect to perturbations in the curvature function $\lambda(y)$. In particular, we show that the solution depends continuously on λ , with the variation controlled by a weighted norm involving the derivative of the relative perturbation. The strategy is to derive the linearized equation for the variation and then apply energy estimates to obtain the desired bounds.

Lemma 7.3 (Linearized Equation). Recall that the governing equation can be written in terms of the operator

$$L_{\lambda}[x] := 2\lambda(s+t)x_{st} + \lambda'(s+t)(x_s+x_t),$$

so that solutions satisfy $L_{\lambda}[x] = 0$. Let x_0 be a solution to the homogeneous Goursat problem corresponding to the coefficient function λ_0 . Consider a perturbed coefficient of the form

$$\lambda(y;\epsilon) = \lambda_0(y) + \epsilon \lambda_1(y),$$

with corresponding solution $x(u, p; \epsilon)$. Then the first-order variation

$$x_1 := \frac{\partial}{\partial \epsilon} x(u, p; \epsilon) \bigg|_{\epsilon=0}$$

satisfies the linear inhomogeneous equation

$$L_{\lambda_0}[x_1] = g(u, p).$$

The forcing term g is given by

$$g(u,p) = -2\lambda_0(u) \frac{d}{du} (\delta \log \lambda) (x_0)_u, \quad \text{with} \quad \delta \log \lambda := \frac{\epsilon \lambda_1(y(u))}{\lambda_0(y(u))}.$$

Proof. The proof follows by linearizing the equation $L_{\lambda}[x] = 0$ with respect to ϵ at $\epsilon = 0$. Since the boundary data for x is fixed, the perturbation x_1 satisfies homogeneous boundary and initial conditions.

We next introduce the function space

$$X_1 := L^{\infty}([c, C]; H^1(I_u)), \text{ with } I_u := [-u, u].$$

To describe the forcing terms, it is convenient to work on the domain

$$\Omega_{c,C} := \{(u,p) \mid c \le u \le C, \ p \in I_u\}.$$

In addition, for any nonnegative measurable weight function $\rho(y)$, we define the weighted L^2 norm

$$||h||_{L^2(\rho(y)\,dy)}^2 := \int_{y_c}^{y_C} |h(y)|^2 \,\rho(y)\,dy,$$

where the endpoints y_c and y_C are determined by $u(y_c) = c$ and $u(y_C) = C$.

We now apply the energy functional from Proposition 7.1 to both the base solution and the first-order variation. With what follows, we denote by $E_0(u)$ the energy of the base solution x_0 , and by $E_1(u)$ the energy of the first-order variation x_1 .

Proposition 7.4 (Linear Stability Estimate). Let x_0 be a C^2 solution for a smooth coefficient $\lambda_0(u)$ and let $E_0(u)$ be its corresponding energy. For a perturbation $\delta\lambda$, the energy $E_1(u)$ of the first-order variation x_1 satisfies the estimate:

$$\sup_{u \in [c,C]} E_1(u) \le M \left(\sup_{u \in [c,C]} E_0(u) \right) \left\| \frac{d}{du} \left(\frac{\delta \lambda}{\lambda_0} \right) \right\|_{L^2(\lambda_0(u)du)}^2,$$

for a constant M that depends on λ_0 and the interval [c, C] but not on the perturbation $\delta\lambda$.

Proof. The proof proceeds in two steps. First, we apply the energy estimate to the solution of the linearized equation, and then we bound the resulting forcing term.

Step 1: The Energy Estimate for x_1 . From Lemma 7.3, x_1 solves the inhomogeneous problem $L_{\lambda_0}[x_1] = g$ with zero initial data, so $E_1(c) = 0$. The energy estimate from Corollary 7.2, applied over the finite interval [c, C], guarantees that the solution's energy is controlled by the L^2 norm of the forcing term:

$$\sup_{u \in [c,C]} E_1(u) \le M_1 ||g||_{L^2(\Omega_C)}^2,$$

where $\Omega_C = \{(s, v - s) \mid c \le v \le C, 0 \le s \le v\}$ and the constant M_1 absorbs the bounded exponential factor from (7.5).

Step 2: Bounding the Forcing Term. We now bound the L^2 norm of g using its definition from Lemma 7.3:

$$||g||_{L^{2}(\Omega_{C})}^{2} = \int_{c}^{C} \int_{0}^{v} \left[-\lambda_{0}(v) \frac{d}{dv} (\delta \log \lambda) \left((x_{0})_{s} + (x_{0})_{t} \right) \right]^{2} ds \, dv$$

$$= \int_c^C \left(\lambda_0(v) \frac{d}{dv} (\delta \log \lambda)\right)^2 \left(\int_0^v \left((x_0)_s(s, v - s) + (x_0)_t(s, v - s)\right)^2 ds\right) dv.$$

We bound the inner integral with the Cauchy–Schwarz inequality:

$$\int_0^v \left((x_0)_s + (x_0)_t \right)^2 ds \le 2 \int_0^v \left((x_0)_s^2 + (x_0)_t^2 \right) ds = \frac{2}{\lambda_0(v)} E_0(v).$$

Substituting this back and pulling out the supremum of the base solution's energy gives

$$||g||_{L^{2}(\Omega_{C})}^{2} \leq \int_{c}^{C} \left(\lambda_{0}(v) \frac{d}{dv} (\delta \log \lambda)\right)^{2} \frac{2E_{0}(v)}{\lambda_{0}(v)} dv$$

$$\leq 2 \left(\sup_{w \in [c,C]} E_{0}(w)\right) \int_{c}^{C} \lambda_{0}(v) \left(\frac{d}{dv} (\delta \log \lambda)\right)^{2} dv.$$

The last term is precisely the squared norm $\left\| \frac{d}{du} (\delta \log \lambda) \right\|_{L^2(\lambda_0(u)du)}^2$. Combining the inequalities gives the final estimate with $M = 2M_1$.

Remark 7.5 (Invariance and Orthogonal Perturbations). The governing equation is invariant under a uniform scaling of the coefficient, $\lambda \mapsto k\lambda$. Our stability estimate reflects this correctly: if $\delta \log \lambda$ is constant, then its derivative vanishes, the forcing term g is zero, and the predicted variation x_1 disappears. It is therefore natural to decompose any perturbation into its mean and a mean-free part,

$$\delta \log \lambda = \overline{\delta \log \lambda} + (\delta \log \lambda)_{\text{ortho}}.$$

Since the mean contributes nothing, the estimate can be expressed in terms of the orthogonal component:

$$||x_1||_{X_1} \le M||x_0||_{X_1} \left\| \frac{d}{dy} \left((\delta \log \lambda)_{\text{ortho}} \right) \right\|_{L^2(\lambda_0(y)dy)}.$$

This makes explicit that stability of the solution depends only on changes to the "shape" of $\log \lambda(y)$, not on uniform rescaling.

8. Conclusions and Future Directions

The study of surfaces with negative curvature has revealed fundamental connections between geometry, analysis, and physical models of thin elastic sheets. In this work, we focused on the hyperbolic Monge–Ampère equation in strip-like geometries, motivated both by its geometric role as the prescribed Gauss curvature equation and by its analytic formulation of localized negative curvature that decays at infinity.

A particularly interesting feature of our problem is that the hodograph transformation reveals a fundamental and irreversible "arrow of time", in contrast to the standard undamped wave equation, whose dynamics are time-reversible. This asymmetry is first dictated at the geometric level: if one attempts to prescribe Cauchy data on a "near" boundary (i.e., for large u = s + t = C) together with Goursat data on the axes, characteristics intersect the boundary at two distinct points, producing over-determined

and inconsistent data. Hence, the geometry forces the problem to be posed with Cauchy data in the "far field" (i.e., for small u = s + t = c), where the boundary uniquely determines the causal past of each point.

This geometric necessity is then confirmed by the energy analysis. The physical decay of curvature requires positive damping $(\lambda'(u) > 0)$ in the hodograph PDE, so that evolution away from the far-field boundary is a stable, forward-in-time process. In contrast, solving in the reverse direction is ill-posed, with the energy identity showing exponential amplification of errors. Together, these arguments provide a two-fold justification in both the geometric and analytic directions of the problem. In addition, they motivate the use of hodograph weak solutions, for which we established well-posedness via a parametrix-corrector method and a detailed analysis of the associated Volterra integral equation.

The results obtained in this article suggest several possible directions for future work:

- Criteria for Fold-Free Solutions and Stability. A crucial next step is to find sufficient conditions on the Cauchy-Goursat data $\{g,h,f,n\}$ and the coefficient $\lambda(u)$ that guarantee a fold-free solution, defining the precise parameter space for physically realizable smooth surfaces. A related goal is to develop a nonlinear stability theory, showing that the property of being fold-free is preserved under small perturbations.
- Sharper Regularity Theory. A complementary direction is to sharpen the regularity theory for these solutions. This would involve investigating how stronger H^k -compatibility conditions on the boundary data can be propagated into the domain to obtain higher-order energy estimates and, under additional assumptions on the data, establish the existence of smooth C^k solutions.
- Self-Similar Solutions and Asymptotic States. The semiinfinite cylinder case invites a search for self-similar solutions, which often act as attractors for a large class of initial data in hyperbolic systems. Finding such solutions and proving their stability would be a major step in understanding the universal, long-term ("large y") asymptotic geometry of these surfaces.
- Numerical Implementation. The parametrix-corrector decomposition is not just an analytical tool; it provides a powerful blueprint for numerical computation. Developing a numerical scheme based on this decomposition would allow for the efficient and accurate computation of solutions, as the parametrix analytically resolves the corner singularity, leaving a more regular problem for the corrector that is amenable to standard numerical methods.
- Broader Generalizations. Further extensions include allowing the curvature function $\lambda(x,y)$ to depend on both spatial variables, which would broaden the class of admissible geometries while posing

new analytic challenges. Another avenue is the study of homogenization problems, where rapidly oscillating coefficients in λ could lead to effective large-scale behavior with both theoretical and applied significance.

• The Rigidity-Flexibility Transition. Perhaps the most significant direction is to investigate the transition from the rigid to the flexible regime. This would involve studying whether solutions, when "pushed", develop the branch point defects that characterize the intricately wrinkled surfaces seen in nature. Such an analysis would provide a direct, unifying link between the two sides of the rigidity-flexibility dichotomy.

ACKNOWLEDGMENTS

SCV was supported in part by NSF awards DMS-2108124 and DMS-2511503. SCV gratefully acknowledges John Gemmer for valuable discussions.

References

- [1] A. ALEXANDROV, Existence and uniqueness of a convex surface with a given integral curvature, C. R. (Doklady) Acad. Sci. URSS (N.S.), 35 (1942), pp. 131–134.
- [2] R. Baker and C. J. L. Doran, Jet bundles and the formal theory of partial differential equations, in Applications of Geometric Algebra in Computer Science and Engineering, L. Dorst, C. Doran, and J. Lasenby, eds., Birkhäuser Boston, Boston, MA, 2002, pp. 133–143.
- [3] Y. F. Borisov, Irregular surfaces of the class $C^{1,\beta}$ with an analytic metric, Sibirsk. Mat. Zh., 45 (2004), pp. 25–61.
- [4] D. Brander, Pseudospherical surfaces with singularities, Ann. Mat. Pura Appl. (4), 196 (2017), pp. 905–928.
- [5] R. L. BRYANT, S.-S. CHERN, R. B. GARDNER, H. L. GOLDSCHMIDT, AND P. A. GRIFFITHS, Exterior differential systems, vol. 18, Springer Science & Business Media, 2013.
- [6] W. CAO AND D. INAUEN, Rigidity and flexibility of isometric extensions, Commentarii Mathematici Helvetici, 99 (2023), pp. 39–80.
- [7] W. CAO AND L. SZÉKELYHIDI, Very weak solutions to the two-dimensional Monge-Ampère equation, Science China Mathematics, 62 (2019), pp. 1041–1056.
- [8] S. CONTI, C. DE LELLIS, AND L. SZÉKELYHIDI, JR., h-principle and rigidity for C^{1,α} isometric embeddings, in Nonlinear partial differential equations, vol. 7 of Abel Symp., Springer, Heidelberg, 2012, pp. 83–116.
- [9] R. COURANT AND D. HILBERT, Methods of Mathematical Physics, Vol. II: Partial Differential Equations, Interscience Publishers, New York, english ed., 1962.
- [10] N. V. Efimov, Generation of singularities on surfaces of negative curvature, Matematicheskii Sbornik, 106 (1964), pp. 286–320.
- [11] Y. ELIASHBERG AND N. MISHACHEV, *Introduction to the h-principle*, vol. 48 of Graduate Studies in Mathematics, American Mathematical Society, Providence, RI, 2002.
- [12] L. C. EVANS, Partial differential equations, vol. 19 of Graduate Studies in Mathematics, American Mathematical Society, Providence, RI, second ed., 2010.
- [13] J. Gemmer, E. Sharon, T. Shearman, and S. C. Venkataramani, *Isometric immersions, energy minimization and self-similar buckling in non-Euclidean elastic sheets*, Europhysics Letters, 114 (2016), p. 24003.

- [14] J. GEMMER AND S. C. VENKATARAMANI, Shape transitions in hyperbolic non-Euclidean plates, Soft Matter, 9 (2013), pp. 8151–8161.
- [15] M. Gromov, Partial differential relations, vol. 9 of Ergebnisse der Mathematik und ihrer Grenzgebiete (3) [Results in Mathematics and Related Areas (3)], Springer-Verlag, Berlin, 1986.
- [16] L. HÖRMANDER, The analysis of linear partial differential operators. I, Classics in Mathematics, Springer-Verlag, Berlin, 2003. Distribution theory and Fourier analysis, Reprint of the second (1990) edition [Springer, Berlin].
- [17] C. Huang, Z. Wang, D. Quinn, S. Suresh, and K. J. Hsia, Differential growth and shape formation in plant organs, Proceedings of the National Academy of Sciences, 115 (2018), pp. 12359–12364.
- [18] T. A. IVEY AND J. M. LANDSBERG, Cartan for beginners: differential geometry via moving frames and exterior differential systems, vol. 61 of Graduate Studies in Mathematics, American Mathematical Society, Providence, RI, 2003.
- [19] R. Kress, Linear Integral Equations, vol. 82 of Applied Mathematical Sciences, Springer, New York, 3rd ed., 2014.
- [20] N. H. KUIPER, On C¹-isometric imbeddings. I, II, Indag. Math., 17 (1955), pp. 545–556, 683–689. Nederl. Akad. Wetensch. Proc. Ser. A 58.
- [21] M. LEWICKA, The Monge-Ampère system: convex integration in arbitrary dimension and codimension, SIAM Journal on Mathematical Analysis, 57 (2025), pp. 601–636.
- [22] ——, The Monge-Ampère system: convex integration with improved regularity in dimension two and arbitrary codimension, Differential and Integral Equations, 38 (2025), pp. 141–174.
- [23] M. LEWICKA AND M. R. PAKZAD, Convex integration for the Monge-Ampère equation in two dimensions, Analysis & PDE, 10 (2017), pp. 695-727.
- [24] M. LEWICKA AND M. REZA PAKZAD, Scaling laws for non-Euclidean plates and the W^{2,2} isometric immersions of Riemannian metrics, ESAIM: Control, Optimisation and Calculus of Variations, 17 (2011), pp. 1158–1173.
- [25] J. NASH, C¹ isometric imbeddings, Annals of mathematics, (1954), pp. 383–396.
- [26] E. G. Poznyak, Isometric immersions of two-dimensional riemannian metrics in euclidean space, Russian Mathematical Surveys, 28 (1973), p. 47.
- [27] E. Sharon, M. Marder, and H. L. Swinney, Leaves, flowers, and garbage bags: making waves, American Scientist, 92 (2004), pp. 254–261.
- [28] E. Sharon, B. Roman, M. Marder, G.-S. Shin, and H. L. Swinney, *Buckling cascades in free sheets*, Nature, 419 (2002), pp. 579–579.
- [29] E. Sharon, B. Roman, and H. L. Swinney, Geometrically driven wrinkling observed in free plastic sheets and leaves, Phys. Rev. E, 75 (2007), p. 046211.
- [30] T. L. Shearman and S. C. Venkataramani, Distributed branch points and the shape of elastic surfaces with constant negative curvature, Journal of Nonlinear Science, 31 (2021), p. 13.
- [31] D. Spring, Convex integration theory, Modern Birkhäuser Classics, Birkhäuser/Springer Basel AG, Basel, 2010. Solutions to the h-principle in geometry and topology, Reprint of the 1998 edition.
- [32] J. J. STOKER, Differential geometry, Wiley Classics Library, John Wiley & Sons Inc., New York, 1989. Reprint of the 1969 original, A Wiley-Interscience Publication.
- [33] F. G. TRICOMI, Integral equations, Dover Publications, Inc., New York, 1985. Reprint of the 1957 original.
- [34] G. B. Whitham, Linear and Nonlinear Waves, John Wiley & Sons, 1974.
- [35] K. Yamamoto, T. Shearman, E. Struckmeyer, J. Gemmer, and S. Venkataramani, *Nature's forms are frilly, flexible, and functional*, European Physical Journal E, 44 (2021).

(M. Deliyianni) Department of Mathematics, University of Arizona, 617 N. Santa Rita Ave., Tucson, AZ 85721

 $Email\ address: \verb|mdeliy1@arizona.edu||$

(S. C. Venkataramani) Department of Mathematics, University of Arizona, 617 N. Santa Rita Ave., Tucson, AZ 85721

 $Email\ address \hbox{: } \mathtt{shankar@arizona.edu}$